# Differences in carbon isotope discrimination between angiosperm and gymnosperm woody plants, and their relationship to atmospheric $O_2$:$CO_2$ ratio, physiology, and environment

Vincent J. Hare[a,b,*], Aliénor Lavergne[b]

[a] *Stable Light Isotope Laboratory, Department of Archaeology, University of Cape Town, South Africa*

[b] *Carbon Cycle Research Group, Department of Physics, Imperial College London, UK*

**Abstract**

For most of the Phanerozoic Eon, Earth's woody vegetation has been dominated by $C_3$ plants – predominantly gymnosperms - with angiosperms only emerging as the dominant plant group as $CO_2$ declined during the Cenozoic (66 Ma onward). At present, differences in carbon isotope discrimination ($\Delta^{13}C$) between angiosperm and gymnosperm plants are relatively small (2–3 ‰), but an increasing body of evidence points to larger differences across geological times (up to 6–7 ‰), potentially associated with varying environmental conditions and atmospheres (i.e. concentrations of atmospheric carbon dioxide, [$CO_2$], and oxygen, [$O_2$] could have ranged from $\sim$ 180 to 1100 ppm, and $\sim$ 15 to 25 %, respectively, across the past 250 Ma). Yet, differences in $\Delta^{13}C$ between the two plant groups, and their potential link to climatic and environmental changes, have not yet been fully explored and understood. Here, we combine a comprehensive *ab initio* model of discrimination, with a recent model of plant eco-physiology based on least-cost optimality theory, to show how differences in $\Delta^{13}C$ between angiosperms and gymnosperms arise. We train the comprehensive model using a very large ($n > 7000$) database of leaf and tree ring data spanning the past 110 years. We find that averaged differences in $\Delta^{13}C$ between angiosperm and gymnosperms decrease modestly with atmospheric [$O_2$]:[$CO_2$] ratios, and increase strongly with vapor pressure deficit ($D$). These relationships can be explained by three key physiological differences: (1) the ratio of cost factors for transpiration to carboxylation (higher in angiosperms); (2) the ratio of mesophyll to stomatal conductances of $CO_2$ (lower in gymnosperms); and (3) differences in photorespiration. In particular, the amount of $CO_2$ released from photorespiration per oxygenation reaction, $\lambda$, is generally lower in gymnosperms than in angiosperms. As a result of these factors, $\Delta^{13}C$ is more sensitive to [$CO_2$] in angiosperms, and to $D$ in gymnosperms. We propose a simplified empirical model to account for this behaviour, and test it against isotopic data from leaves, tree rings and previously-published plant chamber experiments, along with geological data from the Cenozoic. Overall, these data agree with our model over range of [$O_2$]:[$CO_2$] ratios from 100 to 650 mol mol$^{-1}$ (equivalent to a $CO_2$ range around $323 - 525$ ppm at 21% $O_2$), and $D$ levels between 0.45 and 1.1 kPa ($R^2$ = 0.51, RMSE = 0.538‰). Our simplified empirical model offers a new explanation for secular trends in the geological record, and suggests a way

*Corresponding author
*Email address:* vincent.john.hare@gmail.com (Vincent J. Hare)

forward to improve paleo-[$CO_2$] proxies based on terrestrial discrimination models by incorporating the effects of [$O_2$], phylogeny, and photorespiration. Lastly, the framework predicts that the average difference in $\Delta^{13}C$ between woody $C_3$ plant groups will increase in the future if both [$CO_2$] and global $D$ continue to rise as suggested by projections.

*Keywords:* carbon isotope discrimination - $C_3$ photosynthesis - gymnosperms - angiosperms - atmospheric $CO_2$ - atmospheric $O_2$ - paleo-proxies

---

## 1. Introduction

During photosynthesis, terrestrial plants fix atmospheric carbon dioxide ($CO_2$) into the simple sugars they need to grow, a process which sustains almost all life on Earth. In all vascular $C_3$ plants, $CO_2$ first enters the leaf through the stomata, before diffusing to the sites of carboxylation in the chloroplast. At each step along the pathway of carbon from the atmosphere to the leaf sugars, plants discriminate strongly against the heaviest stable carbon isotope ($^{13}C$), leading to a substantial difference between the stable carbon isotope compositions ($\delta^{13}C$) of the source atmospheric $CO_2$ ($\delta^{13}CO_2$), and of the carbon fixed within the leaf ($\delta^{13}C_{leaf}$). This difference is commonly defined as the leaf-level carbon isotopic discrimination (referred to $\Delta^{13}C$) and expressed in per mil (‰) as:

$$\Delta^{13}C = \frac{\delta^{13}CO_2 - \delta^{13}C_{leaf}}{1 + \delta^{13}C_{leaf}/1000} \quad (1)$$

The two dominant groups of woody $C_3$ plants, i.e. angiosperms and gymnosperms, have different physiological traits, including distinct vascular structures and reproductive habits (e.g. exposed seeds versus seeds enclosed in fruit). There are also subtle, yet significant, differences in $\Delta^{13}C$ between the two plant groups. Globally, modern leaf isotope data (e.g. Diefendorf et al. (2010)) show that angiosperms are 2-3 ‰ more depleted in $^{13}C$ than gymnosperms (see Fig. 1). This isotopic offset is observed in pre-industrial wood cellulose (Stuiver and Braziunas, 1987) and in modern tree rings of the same age growing in the same location and thus under the same conditions of evaporative demand and soil water availability (Leavitt and Newberry, 1992), which suggests that differences in $\Delta^{13}C$ levels are primarily driven by physiology, as opposed to environment. However, this is clearly not always the case as the $\Delta^{13}C$ offset tends to decrease with latitude/temperature gradients (Leavitt and Newberry, 1992; Stuiver and Braziunas, 1987; Pedentchouk et al., 2008). No single clear physiological or environmental factor is therefore responsible for differences in $\Delta^{13}C$ between angiosperm and gymnosperm plants, and the reasons for the observed isotopic offsets between the two plant groups are yet to be fully explored and understood.

In addition to these factors, $\Delta^{13}C$ values in gymnosperm and angiosperm plants are sensitive to changing atmospheric composition. Several emerging lines of evidence from $\delta^{13}C$ data derived from tree rings (Voelker et al., 2016), cellulose and faunal collagen (Hare et al., 2018), species-specific lipid biomarkers (Schouten et al., 2007), and speleothems (Breecker, 2017), suggest that $\Delta^{13}C$ in angiosperms and gymnosperms has responded differently to past changes in atmospheric $CO_2$ concentration (hereafter [$CO_2$]). Chamber experiments have also shown clear effects of changing $O_2$ concentration, [$O_2$], on $\Delta^{13}C$, depending on $C_3$ phylogeny (Porter et al., 2017). Atmospheric [$O_2$]:[$CO_2$] ratios have varied substantially since the radiation of gymnosperms in the Mesozoic Era (252

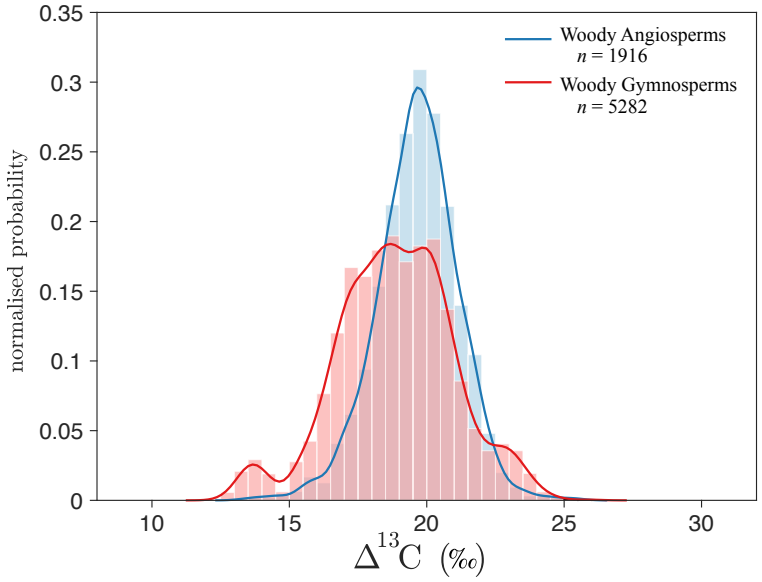


Figure 1: Distribution of carbon isotope discrimination in $C_3$ woody angiosperm and gymnosperm plants, compiled from global bulk leaf and tree ring cellulose records (see Methods). Note: In this figure, tree ring cellulose $\delta^{13}C$ values are corrected for post-photosynthetic fractionation by the subtraction of 2.1‰.

- 66 Ma), when [$CO_2$] was high ($>$ 1000 ppm). During these times, [$O_2$] was generally higher than present-day values of 21 %, perhaps as high as 29 % (Mills et al., 2016). As [$CO_2$] declined over the Cenozoic (66 Ma onwards), angiosperms rapidly diversified to become the dominant land plant group. It is thought that the radiation of angiosperms coincided with important evolutionary adaptations to lower [$CO_2$] within this plant group; including a higher mesophyll conductance to $CO_2$, denoted $g_m$ (Yiotis and McElwain, 2019; Flexas and Carriquí, 2020), an increased vein density (De Boer et al., 2012), and more efficient stem hydraulic properties (Zanne et al., 2014). Concentrations of atmospheric $CO_2$ regularly reached their geological minima, ∼180 ppm, during the Pleistocene ice ages (2.58 Ma to 11.7 ka) (Bereiter et al., 2015). Taken together, the full geological range of [$O_2$]:[$CO_2$] ratios experienced by both gymnosperms and angiosperms over the Cenozoic is between approximately 150 mol mol$^{-1}$ (Paleocene-Eocene Thermal Maximum, PETM; $\sim$ 56 Ma) and 1150 mol mol$^{-1}$ (Last Glacial Maximum, LGM; 21 ka). This is a substantial range, and it is possible that these atmospheric changes led to differences in $C_3$ plant discrimination, although the exact magnitudes of group-specific responses remain uncertain.

In geological contexts, it is generally assumed that isotope discrimination in $C_3$ plants is independent of phylogeny. This implies that the offset in $\Delta^{13}C$ between angiosperms and gymnosperms is more or less constant over time. As a result, offsets of 2-3‰ between ancient tissues from each plant group are sometimes regarded as indications of fossil integrity, i.e. resistance to diagenesis (Diefendorf et al., 2015; Schlanser et al., 2020a). However, emerging evidence suggests that isotope discrimination might vary between different $C_3$ plant groups (Sheldon et al., 2020), and substantial changes in the difference of $\Delta^{13}C$ values between angiosperms and gymnosperms are occasionally observed in the geological record. For instance, this offset ranged from less than -3 ‰ (Diefendorf et al., 2015) to greater than +4 ‰ (Schouten et al., 2007; Schlanser et al., 2020a) before, during, and after the extreme climate states of the PETM. Some of these changes have been explained by differences in plant water-use efficiency (WUE),

i.e. the ratio of carbon assimilated to water transpired, which is intrinsically coupled to leaf-level discrimination (Soh et al., 2019; Lavergne et al., 2019). On the other hand, they could also be explained by diagenesis, or variability in post-photosynthetic fractionations, particularly in the case of plant lipids (Diefendorf et al., 2019). Underlying all these explanations, it is also plausible that a substantial proportion of these changes was driven by fundamental physiological differences between the two plant groups, modulated by atmospheric $[O_2]$:$[CO_2]$ ratios. Thus, no satisfactory unifying framework yet exists to explain the variability observed in the geological record; a full understanding of the drivers responsible for the different plant responses between $C_3$ groups is still needed.

The aim of this study is to propose a model for isotope discrimination in $C_3$ plants that can account for differences in phylogeny, and that can reasonably explain variations in the geological record. First, we examine the impact of plant physiology on $\Delta^{13}C$ among the two groups by combining a comprehensive *ab initio* model of leaf discrimination, with a stomatal model based on the least-cost optimality hypothesis (Prentice et al., 2014). The optimal model has been used for exploring stomatal responses to the environment as recorded in modern isotopic samples derived from $C_3$ plants (Wang et al., 2017; Lavergne et al., 2020a), but its application to geological timescales is novel. We then train the coupled stomatal-discrimination model against a large literature compilation of $\Delta^{13}C$ measures derived from tree ring and leaf samples spanning the $20^{th}$ century to identify the key parameters that give rise to the different physiological responses between angiosperms and gymnosperms. We then investigate how the difference in $\Delta^{13}C$ values between the two plant groups can be explained and predicted from environmental factors such as vapor pressure deficit ($D$), and from changes in atmospheric $[O_2]$:$[CO_2]$ ratios. We then compare our predictions with isotopic data derived from leaves, tree-rings, plant chamber experiments, and ultimately geological data.

Finally, we discuss the implications of our findings for the interpretation of the geological record and for the reconstruction of paleo-$[CO_2]$. Models of $C_3$ carbon isotope discrimination are routinely used to estimate paleo-$[CO_2]$ (Schubert and Jahren, 2012; Cui et al., 2020; Franks et al., 2014), but seldom account for differences between plant groups, changes in $D$, or $[O_2]$ levels over time - although all three effects might influence terrestrial paleo-proxies (Porter et al., 2019; Hollis et al., 2019) and thereby affect estimates of the (paleo)climate sensitivity - the amount of warming experienced after a doubling of $[CO_2]$ during geological times. Thus, our findings may ultimately contribute to ongoing efforts to better constrain paleo-$[CO_2]$ reconstructions and thus predict more accurately the (paleo)climate sensitivity.

## 2. Theory

Farquhar et al. (1982) proposed a mathematical description of the discrimination against $^{13}C$, based on a model used to describe the biochemistry of $CO_2$ assimilation in $C_3$ leaves - the 'FvCB' model (Farquhar et al., 1980). Both the FvCB model and the corresponding discrimination model are foundational to our understanding of $C_3$ photosynthesis, having been applied to a wide range of scientific questions in plant eco-physiology, paleoecology and geochemistry. In addition, the FvCB model has been widely used in Earth System modeling to predict the rate

of carbon assimilation (A) by plants, and thus to study the carbon cycle. A comprehensive *ab initio* description of bulk leaf discrimination derived from Farquhar et al. (1982) can be written following Busch et al. (2020):

$$\begin{aligned}\Delta^{13}\mathrm{C} = &\frac{1}{1-t}\left[a_\mathrm{b}\frac{C_\mathrm{a}-C_\mathrm{s}}{C_\mathrm{a}} + a_\mathrm{s}\frac{C_\mathrm{a}-C_\mathrm{s}}{C_\mathrm{a}}\right] \\ &+ \frac{1+t}{1-t}\left[a_\mathrm{m}\frac{C_\mathrm{i}-C_\mathrm{c}}{C_\mathrm{a}} + b\frac{C_\mathrm{c}}{C_\mathrm{a}} - \frac{R_\mathrm{d}}{A}\frac{\alpha_\mathrm{b}}{\alpha_\mathrm{e}\alpha_\mathrm{R}}e\frac{C_\mathrm{c}}{C_\mathrm{a}} - \frac{\alpha_\mathrm{b}}{\alpha_\mathrm{f}\alpha_\mathrm{R}}\frac{\Gamma^*}{C_\mathrm{a}}\left(f - wh\right)\right]\end{aligned} \tag{2}$$

$C_\mathrm{a}$, $C_\mathrm{s}$, $C_\mathrm{i}$, and $C_\mathrm{c}$ are the concentrations of $CO_2$ along the $CO_2$ diffusion pathway, i.e., in the atmosphere, the leaf surface, the intercellular space and the chloroplast, respectively, while $a_\mathrm{b}$, $a_\mathrm{s}$, $a_\mathrm{m}$, and $b$, are the fractionations associated with the $CO_2$ diffusion though the boundary layer (2.9‰), stomata (4.4‰), and mesophyll (1.8‰), and carboxylation by the enzyme Rubisco (30‰), respectively. The values for the fractionations are relatively well-constrained from theory (Craig, 1954) as well as *in vitro* experiments and molecular dynamics simulations (see discussion in Ubierna and Farquhar (2014)). By comparison, the fractionations due to mitochondrial respiration, $e$, and photorespiration, $f$, are relatively poorly constrained. $e$ is often regarded as negligible (e.g. Ghashghaie et al. (2003)), and literature values of $f$ range from 7 to 16‰, with a theoretical value of around 11‰ (Tcherkez, 2006).

$h$ is the apparent fractionation associated with several processes such as starch formation, and the export of 3-phosphoglyceraldehyde (3-PG) and is currently difficult to constrain (Busch et al., 2020). $w$ is a factor given by $(6C_\mathrm{c} + 9\Gamma^*)/(5C_\mathrm{c} + 10\Gamma^*)$, which is approximately 1.1, at typical values of $C_\mathrm{c}$ and $\Gamma^*$. $t$ is the ternary correction factor depending on the rate of transpiration and the conductance to $CO_2$ diffusion in air (Farquhar and Cernusak (2012)), and $\alpha_i$ values ($i = \mathrm{a},\ \mathrm{b},\ \mathrm{f},\ \mathrm{and}\ \mathrm{e}$) are the formal fractionation factors associated with the respective processes (i.e., diffusion, carboxylation, mitochondrial respiration and photorespiration, respectively). $R_\mathrm{d}$ is the rate of mitochondrial respiration and $\Gamma^*$ is the photorespiratory compensation point in absence of mitochondrial respiration, i.e., the value of $C_\mathrm{i}$ at which the rate of photosynthetic $CO_2$ uptake equals that of photorespiratory $CO_2$ evolution. A full list of variables, and their respective definitions, can be found in Table 1.

In its full form, Eqn. (2) is not easily applied to the geological record because of uncertainties in the values of some terms in the equation. Assuming that both ternary and respiration effects are negligible ($t \approx 0$ and $e \approx 0$) and that $\alpha_i \approx 1$, Ubierna and Farquhar (2014) proposed the following approximation that is applicable in a broad range of environmental conditions:

$$\Delta^{13}\mathrm{C} = a_\mathrm{s}(1-\chi) + a_\mathrm{m}(\chi - \chi_\mathrm{c}) + b\chi_\mathrm{c} - (f - wh)\frac{\Gamma^*}{C_\mathrm{a}} \tag{3}$$

where we adopt the notation $\chi = C_\mathrm{i}/C_\mathrm{a}$, and $\chi_\mathrm{c} = C_\mathrm{c}/C_\mathrm{a}$. Note that we have slightly modified the original equation to retain the $w$ and $h$ terms proposed by Busch et al. (2020). This equation is more mathematically tractable than Eqn. (2), and accurate for a first order understanding of plant $\Delta^{13}\mathrm{C}$, because it includes fractionations associated with photorespiration and $CO_2$ diffusion in the mesophyll which are critical for reproducing the observed global trends in atmospheric $\delta^{13}\mathrm{C}$ during the $20^{th}$ century (Keeling et al., 2017). The non-negligible photorespiratory effect on the discrimination is also increasingly acknowledged in geological studies (Schubert and Jahren, 2018; Zhang et al., 2019; Porter et al., 2019). At current $CO_2$ levels (∼410 ppm), the photorespiration term in Eqn. (3)

contributes only slightly to isotope discrimination, e.g. $< 1‰$ at a typical $\Gamma^*$ of $\sim 3.2$ Pa, at 20 $^o$C (value from Bernacchi et al. (2002)), assuming $h$ is negligible. However, its contribution increases at lower $CO_2$ concentrations, and/or higher $\Gamma^*$ (higher leaf temperature). Because Rubisco has an affinity for both $O_2$ and $CO_2$, $\Gamma^*$ also depends on the oxygen concentration in the chloroplast, $O_c$, and on the amount of $CO_2$ released from photorespiration per oxygenation reaction - a variable defined by Busch (2020) as $\lambda$. The relationship between these variables can be written as:

$$\Gamma^* = \frac{\lambda O_c}{S_{c/o}} \tag{4}$$

where $S_{c/o}$ is the Rubisco specificity factor. Emerging studies (e.g. Busch et al. (2018)) have shown that $\lambda$ depends on the relative proportions of glycine and 5,10-methylene tetrahydrofolate ($CH_2$-THF) exported from the photorespiratory pathway. Glycine is an important building block of compounds manufactured by plants under stress, and $CH_2$-THF is the chemical precursor of lignin and many other secondary products. Typically, $\lambda$ is around 0.5 (corresponding to 25% of the 2-phosphoglycerate carbon lost as $CO_2$), but as the relative proportion of these components change, so too does $\lambda$ - and the discimination against $^{13}$C due to photorespiration.

Incorporating mesophyll effects, and retaining the photorespiration terms (see full derivation in Electronic Annexure), Eq. (3) can be rewritten more succinctly as:

$$\Delta^{13}C = \bar{a} + \big[b - \bar{a}\big]\chi_c - (f - wh)\frac{\Gamma^*_c}{C_a} \tag{5}$$

where $\bar{a} = (a_s\theta_m + a_m)/(1 + \theta_m)$ and $\theta_m$ is the ratio of mesophyll conductance to stomatal conductance ($g_m/g_s$). $\bar{a}$ thus represents all the fractionation processes during the $CO_2$ diffusion along the pathway from the atmosphere to the site of photosynthesis (chloroplast). Note that if the photorespiration is assumed negligible, and the mesophyll conductance is assumed infinite (i.e. $\chi_c = \chi$), Eqn. (5) can be rewritten as: $\Delta^{13}C \approx a_s + (b - a_s)\chi$. This simple formulation has been widely used in the literature for modern and paleo studies (see also Lavergne et al. (2019), and Hare et al. (2018)).

Eqn. (5) offers a more complete formalism than its simplest version, but lacks an expression for the $\chi_c$ term. A theoretical model for $\chi_c$ was recently derived by Wang et al. (2017) using an evolutionary optimality approach that assumes that $C_3$ land plants minimise the summed unit costs of transpiration and carboxylation. In this framework, $\chi_c$ depends on $C_a$, the daytime leaf temperature ($T_d$, °C), the leaf-to-air vapour pressure deficit ($D$, kPa), and the ratio of cost factors for carboxylation to transpiration at 25 °C ($\beta_c$, unitless), as:

$$\chi_c = \frac{\Gamma^*_c}{C_a} + \big(1 - \frac{\Gamma^*_c}{C_a}\big)\frac{\xi_c}{\xi_c + \sqrt{D}} \tag{6}$$

where

$$\xi_c^2 = [\beta_c(K + \Gamma^*_c)]/[1.6\eta^*(1 + 1/\theta_m)] \tag{7}$$

Table 1: List of symbols used in this study, and their definitions.

| Variables (units) | Description | Refs. |
|---|---|---|
| $\Delta^{13}$C (‰) | leaf-level carbon isotope discrimination | 1,2,3 |
| $\Delta^{13}C^{*}_{a-g}$ (‰) | difference between average co-located angiosperm and gymnosperm $\Delta^{13}$C at constant $T_d$, $P_{atm}$, & $D$ | *this study* |
| $\varepsilon_{lipid}$ (‰) | post-photosynthetic fractionation during biosynthesis of leaf lipids | 4,5 |
| $\varepsilon_{cellulose}$ (‰) | post-photosynthetic fractionation during biosynthesis of cellulose | 6,7 |
| $t$ | ternary correction factor | 1,2,3 |
| $a_s$, $a_m$ (‰) | fractionations for $CO_2$ diffusion in air, 4.4‰, and water, 1.8‰ | 8,1 |
| $b$ (‰) | fractionation during Rubisco carboxylation, 30‰ | 1 |
| $f$ (‰) | fractionation during photorespiration, 8-18‰ (theoretical: 11‰) | 9 |
| $h$ (‰) | apparent fractionation resulting from starch formation, and/or the kinetic fractionation associated with the export of triose phosphates (TP) from the chloroplast, and/or enzymes such as aldolase, transaldolase, transketolase and TP isomerase | 3 |
| $w$ (unitless) | coefficient of $h$ in $f - wh$ | 3 |
| $\alpha_b$; $\alpha_e$; $\alpha_f$ (unitless) | fractionation factors for $^{13}$C/$^{12}$C during carboxylation $\alpha_b = 1+b$; respiration $\alpha_e = 1+e$; photorespiration $\alpha_f = 1 + f$ | 1 |
| $\alpha_h$ (unitless) | as above, for $h$ | 3 |
| $\lambda$ (unitless) | amount of $CO_2$ released from photorespiration per oxygenation reaction, relative to that of *N. tabacum* at 25°C ($\lambda_{ref}$) | 10 |
| $\lambda_a$, $\lambda_g$ (unitless) | average $\lambda$, woody angiosperms, woody gymnosperms | *this study* |
| $\varepsilon_f$ (unitless) | gradient of the slope of $\Delta^{13}C^{*}_{a-g}$ vs [$O_2$]/[$CO_2$] at constant $T_d$ | *this study* |
| $\varepsilon_{ab}$ (unitless) | gradient of the slope of $\Delta^{13}C^{*}_{a-g}$ vs $D$ at constant $T_d$ | *this study* |
| $\alpha_G$; $\alpha_T$ (unitless) | proportion of glycine removed from the photorespiratory pathway; proportion of 2-Phosphoglycolate carbon exported as $CH_2$-THF from the photorespiratory pathway | 11,10 |
| $C_a$ (Pa) | atmospheric p$CO_2$ (Pa), or as concentration ($\mu$mol mol$^{-1}$) | |
| $C_s$ (Pa) | leaf-surface p$CO_2$ (Pa), or as concentration ($\mu$mol mol$^{-1}$) | |
| $C_i$ (Pa) | leaf intercellular p$CO_2$ (Pa), or as concentration ($\mu$mol mol$^{-1}$) | |
| $C_c$ (Pa) | chloroplastic p$CO_2$ (Pa), or as concentration ($\mu$mol mol$^{-1}$) | |
| $O_c$ (mol.mol$^{-1}$) | chloroplastic oxygen concentration | |
| $g_s$ (mol m$^{-2}$ s$^{-1}$) | stomatal conductance | 12,13 |
| $g_m$(mol m$^{-2}$ s$^{-1}$) | mesophyll conductance | 12,13 |
| $\beta_c$ (unitless) | ratio of carboxylation to transpiration cost factors at 25 °C | 14 |
| $K_c$ (Pa) | Michaelis-Menten coefficient of Rubisco carboxylation | 15 |
| $K_o$ (Pa) | Michaelis-Menten coefficient of Rubisco oxygenation | 15 |
| $K$ (Pa) | effective Michaelis-Menten coefficient of Rubisco | 15 |
| $\Gamma_c$ (Pa) | chloroplastic $CO_2$ compensation point in the absence of mitochondrial respiration, when $A = 0$ | 2 |
| $\Gamma^*$ (Pa) | chloroplastic $CO_2$ compensation point, absence of mitochondrial respiration, when $A = -\mathcal{R}_d$ | 2 |
| $S_{c/o}$ (mol mol$^{-1}$) | Rubisco $CO_2$/$O_2$ specificity | 16 |
| $T_d$ (°K) | daytime leaf temperature | |
| $D$ (kPa) | daytime vapour pressure deficit | |
| [$O_2$] (mol mol$^{-1}$) | atmospheric oxygen concentration | |
| [$CO_2$] (mol mol$^{-1}$) | atmospheric carbon dioxide concentration | |

1. Ubierna and Farquhar (2014) 2. Ubierna et al. (2019) 3. Busch et al. (2020) 4.Diefendorf et al. (2012) 5. Diefendorf et al. (2019) 6. Frank et al. (2015) 7. Lavergne et al. (2020a) 8. Craig (1954) 9. Tcherkez (2006) 10. Busch (2020) 11. Busch et al. (2018) 12. Flexas and Carriquí (2020) 13. Yiotis and McElwain (2019) 14. Wang et al. (2017) 15. Bernacchi et al. (2002) 16. Galmés et al. (2016)

$\eta^*$ (unitless) is the viscosity of water relative to its value at 25 °C and $K$ (Pa) is the effective Michaelis constant for Rubisco-limited photosynthesis at ambient partial pressure of $O_2$ (Pa). Note that Eqn. (6) implicitly links both $D$ and $C_a$ to plant WUE, via the relationship between $\chi_c$ and intrinsic WUE, i.e. iWUE $= \theta_m/(1+\theta_m)C_a(1-\chi_c)1.6$ (Ehleringer et al., 1993; Soh et al., 2019; Lavergne et al., 2019).

What differences in discrimination are expected between the two $C_3$ plant groups according to this theory? The terms in Equations (5-7) can be divided into three categories: (1) constants associated with kinetic fractionation ($a_s$, $a_m$, $b$, $f$), (2) atmospheric and environmental variables ($D$, $C_a$ and $\eta^*$), and variables associated with the kinetics of Rubisco ($K$ and $\Gamma^*$, both temperature- and atmospheric pressure-dependent); and finally, (3) plant-specific parameters related to vascular/leaf morphology ($\beta_c$ and $g_m/g_s$), and metabolism ($\lambda$). Because Rubisco is common to all oxygenic phototrophs, and is thought to have suffered relatively little modification through geological times, it is reasonable to assume that differences in $\Delta^{13}C$ between $C_3$ plant groups arise from $\beta_c$, $g_m/g_s$ and $\lambda$, modulated by site-specific environmental conditions. These three plant-specific parameters are unitless, and are assumed to be constants, independent of environmental changes.

Here, we first examine the expected values for $\beta_c$, $g_m/g_s$, and $\lambda$ using a large compilation of leaf and tree ring $\Delta^{13}C$ measurements, spanning a wide range of environments. We then perform sensitivity analyses using Eqns. (5-7) to determine the impacts of $T_d$ and $D$ variations on changes in $\Delta^{13}C$, across the full range of Cenozoic [$O_2$]:[$CO_2$] ratios. Finally, we propose a simple empirical model for describing the dependence of the offset in $\Delta^{13}C$ values between angiosperm and gymnosperms upon [$O_2$]:[$CO_2$] ratio, at any given $T_d$ and $D$.

## 3. Methods

### *3.1. Compilation of tree ring and leaf stable carbon isotope measurements*

We used a large global dataset (the "training dataset") of leaf and tree ring $\delta^{13}C$ measurements, developed and partly used elsewhere (Lavergne et al., 2020b), spanning the whole $20^{th}$ century ([$CO_2$] ranging between 297 and 401 ppm). The leaf isotopic dataset was derived from three published compilations (Cornwell et al., 2016; Diefendorf et al., 2010; Sheldon et al., 2020), while the tree ring isotopic dataset was provided by Lavergne et al. (2020a). After removal of duplicate values, we used the TRY database (Kattge et al., 2020) to assign leaf phenology (deciduous/evergreen), plant vascular type (angiosperm/gymnosperm) and woodiness (woody/non-woody plants) to each plant material. We only selected data from $C_3$ woody plants for the analyses (total of $n = 7098$ measurements with $n = 1916$ for angiosperms and $n = 5282$ for gymnosperms). Note that because the theory for $\Delta^{13}C$ is only valid for well-mixed atmospheric $\delta^{13}CO_2$, we excluded data showing the 'canopy effect', i.e. those from tropical closed-canopy locations, and/or $\delta^{13}C$ < -30‰ (i.e. we adjusted the Kohn (2010) cutoff value of -31.5 ‰ by ~1.1‰ to account for the Suess effect). We corrected tree ring $\delta^{13}C$ data for post-photosynthetic fractionations ($\delta^{13}C$ being more depleted in leaves than in tree rings, e.g. Cernusak et al. (2009)) using two different approaches, which we labelled correction "A" and correction "B". Correction "A" assumed a constant value for post-photosynthetic fractionation of $\varepsilon_{cellulose} = -2.1 \pm 1.2$‰ as used in earlier studies (Frank et al., 2015; Lavergne et al., 2020a). Because the factors influencing post-photosynthetic fractionation are currently uncertain (Gessler

et al., 2014), it is also possible that $\varepsilon_{\text{cellulose}}$ varies between plant species. Therefore, correction "B" used averaged estimates of $\varepsilon_{\text{cellulose}}$ caculated from Guerrieri et al. (2016) and Guerrieri et al. (2019) data for each species (if available). The average correction "B" was $\varepsilon_{\text{cellulose,angio}} = -2.8‰$ for angiosperms, and $\varepsilon_{\text{cellulose,gymno}} = -4.7$ ‰ for gymnosperms.

### *3.2. Atmospheric and environmental data*

To calculate $\Delta^{13}C$ from $\delta^{13}C$ values for our training dataset, we used mean annual $\delta^{13}CO_2$ data from Graven et al. (2017). $CO_2$ concentrations were taken from the compilation of Köhler et al. (2017), which is based on a spline interpolation of direct observations (yearly average), and ice core measurements. [$CO_2$] was converted from ppm to Pa using site elevation data obtained from high-resolution sources using the coordinates of the selected sites (e.g. NED1 (USGS) in North America, SRTM1 (NASA) in Europe). For each site, daytime growing season temperature, $T_{\text{d}}$, and vapour pressure deficit, $D$, were calculated from monthly 0.5$^o$ resolution historical climate data provided by the Climatic Research Unit (CRU TS4.03) (Harris et al., 2014). Note that the $T_{\text{d}}$ values were adjusted to leaf values following Helliker and Richter (2008), i.e., sub-tropical to boreal leaf temperatures converging to $21.4 \pm 2.2$ $^o$C. Further details of these calculations can be found in Text S1 of Lavergne et al. (2020b), and in the Electronic Annexure.

### *3.3. Estimation of plant-specific parameters*

To estimate the parameters $\beta_{\text{c}}$, $g_{\text{m}}/g_{\text{s}}$ and $\lambda$, we employed a Markov chain Monte Carlo technique (MCMC) in MATLAB R2017b (Mathworks, Inc.), based on widely-used delayed rejection adaptive Metropolis (DRAM) algorithm of Haario et al. (2006). The approach was chosen because it allowed us to better incorporate prior constraints on parameters (for instance, leaf gas exchange measurements have shown that $g_{\text{m}}/g_{\text{s}}$ in gymnosperms range around 0.5-4.3 (Yiotis and McElwain, 2019)). Parameters for $C_3$ woody angiosperms and gymnosperms were estimated using the training dataset (Section 3.1), but also using the tree ring and leaf data from the training dataset individually (the latter calibrated parameters are reported in the Electronic Annexure). In all cases, we considered a model of the form of Eqns. (5-7), with Gaussian errors, and constants $b = 30‰$, $a_s = 4.4‰$, $a_m = 1.8‰$ (Ubierna and Farquhar, 2014), $R = 8.3145$ J mol$^{-1}$ K$^{-1}$, and $f = 11 \pm 4‰$ (Tcherkez, 2006). In practice, we found that the best fit (lowest RMSE) was obtained using a value of $h = -1$ ‰ for angiosperms, and $h = -10$ ‰ for gymnosperms. Rubisco kinetic parameters measured on tobacco leaves were taken from Bernacchi et al. (2002). The estimated values of $\lambda$ for each plant vascular group were reported relative to that of tobacco at 25$^o$C, denoted $\lambda_{\text{ref}}$. Full details of the fitting procedure, and simulation of Rubisco kinetics, can be found in the Electronic Annexure.

### *3.4. Simulations of plant $\Delta^{13}C$ over variable [$O_2$]:[$CO_2$] ratios, and comparison to tree ring and chamber isotopic data*

We simulated the expected responses of plant $\Delta^{13}C$ to environmental changes across a range of [$O_2$]:[$CO_2$] ratios spanning the Cenozoic era (66 Ma onwards) from ~200 (e.g. Paleogene) to 1200 mol mol$^{-1}$ (e.g. LGM) using Eqns. (5-7) and our best-fit values for $\beta_{\text{c}}$, $g_{\text{m}}/g_{\text{s}}$, and $\lambda/\lambda_{\text{ref}}$. The simulations were performed at 20$^o$C for two

different levels of vapour pressure deficit: low $D$ (0.23 kPa) and high $D$ (1.54 kPa). Although this choice of $D$ levels may seem arbitrary, it encompasses a reasonably wide range of environments (optimal $D \sim 0.8$ kPa).

We then compared our results against our "testing dataset" which was comprised of averaged $\Delta^{13}C$ differences calculated from the tree ring and leaf isotopic compilation, Cenozoic geological data from the available literature sources (Diefendorf et al., 2015; Bechtel et al., 2008, 2019; Schlanser et al., 2020a; Schouten et al., 2007), and the chamber experiments data derived from Porter et al. (2017). The chamber experiments from the latter study were conducted on woody angiosperms and gymnosperms under conditions of variable [$O_2$] and [$CO_2$], i.e. ranging from 16 to 21 % and from 428 to 1916 ppm, respectively. Note that for various reasons, we excluded these data from the training dataset to estimate the plant-specific parameters. These included potential uncertainties in chamber design (Porter et al., 2015), and estimation of chamber $\delta^{13}CO_2$ values (Leavitt, 2001), which occasionally result in high variability of $\Delta^{13}C$. In these previously-published chamber experiments, angiosperm and gymnosperm plants were grown at constant $T_d$ and $D$ (20 $^o$C and 0.82 kPa, respectively). In order to be comparable to our compilation, non-woody species (*Z. aethiopica*) from Porter et al. (2017) were excluded from our analysis, and we selected available tree ring data at the same $T_d$ and $D$ levels. Tree ring data were averaged for [$O_2$]/[$CO_2$] intervals of 10 mol mol$^{-1}$ over the range 200-1200 mol mol$^{-1}$, and for $D$ intervals of 0.5 kPa over the range 0.4-1.0 kPa.

## 4. Results

### *4.1. Plant-specific parameters for woody angiosperms and gymnosperms*

Significant differences between woody angiosperms and gymnosperms are identified in all three plant-specific parameters (see Table 2, Fig. 2). The best-fit values of $\beta_c$ (combining leaf and tree ring datasets, correction "A") are $210 \pm 25$ ($1\sigma$) for angiosperms and $147 \pm 10$ for gymnosperms. The value for angiosperms is in excellent agreement with that obtained by Lavergne et al. (2020b) using robust linear regressions (i.e. $211 \pm 1.8$), but that for gymnosperms is lower than the one obtained by the same study (i.e. $286 \pm 1.6$), and the value first estimated by Wang et al. (2017), i.e. 343.

For both corrections, $g_m/g_s$ is higher in angiosperms (e.g. $2.6 \pm 0.7$) than in gymnosperms (e.g. $0.98 \pm 0.10$), with greater spread in the values for angiosperms. These general trends echo the findings of previous studies (Yiotis and McElwain, 2019; Flexas and Carriquí, 2020) showing higher $g_m$ in angiosperms than in gymnosperms using leaf-gas exchange measurements. For instance, Yiotis and McElwain (2019) found $g_m/g_s$ values in the range $1.8 \pm 1.1$ for angiosperms and $0.9 \pm 0.1$ for gymnosperms, in good agreement with our values. Flexas and Carriquí (2020) found a slightly lower range of 0.8-1.7 for angiosperms (95% CI), but their range of 0.5-1.3 for gymnosperms is also in good agreement with our findings.

The most pronounced differences between the two plant groups are observed for $\lambda/\lambda_{ref}$ (Fig. 2c), with values around 5.2 for angiosperms and 0.1 for gymnosperms. Using species-specific $\varepsilon_{cellulose}$ (correction "B"), $\lambda/\lambda_{ref}$ is slightly higher than using correction "A" for gymnosperms (0.2), but still significantly lower than the comparable value for angiosperms (4.0).

Table 2: Best fit plant-specific parameters for Eqns. (5-7) fitted to global $\Delta^{13}C$ data from leaves and tree rings. Parameters are: $\beta_c$, the ratio of carboxylation to transpiration cost factors at 25$^o$C; $g_m/g_s$, the ratio of mesophyll to stomatal conductance; and $\lambda/\lambda_{ref}$, the amount of $CO_2$ released from transpiration per oxygenation reaction, relative to that of *N. tabacum* at 25$^o$C. All values are unitless, errors are $1\sigma$. Correction "A" used a constant post-photosynthetic fractionation factor for tree ring cellulose, $\varepsilon_{cellulose} = -2.1$ ‰, whereas correction "B" used species-specific post-photosynthetic fractionation factors (i.e., $\varepsilon_{cellulose,angio} = -2.8$‰ for angiosperms and $\varepsilon_{cellulose,gymno} = -4.7$ ‰ for gymnosperms). Lowest RMSE values were found with with $h = -1$‰ for angiosperms, and $h = -10$‰ for gymnosperms.

| | $\beta_c$ | $g_m/g_s$ | $\lambda/\lambda_{ref}$ | RMSE |
|---|---|---|---|---|
| woody angiosperms | | | | |
| Correction "A" | $210 \pm 25$ | $2.6 \pm 0.7$ | $5.2 \pm 0.2$ | 1.436 |
| Correction "B" | $213 \pm 25$ | $2.5 \pm 0.7$ | $4.0 \pm 0.2$ | 1.463 |
| woody gymnosperms | | | | |
| Correction "A" | $147 \pm 10$ | $0.98 \pm 0.10$ | $0.1 \pm 0.1$ | 1.767 |
| Correction "B" | $281 \pm 18$ | $0.93 \pm 0.10$ | $0.2 \pm 0.2$ | 2.140 |

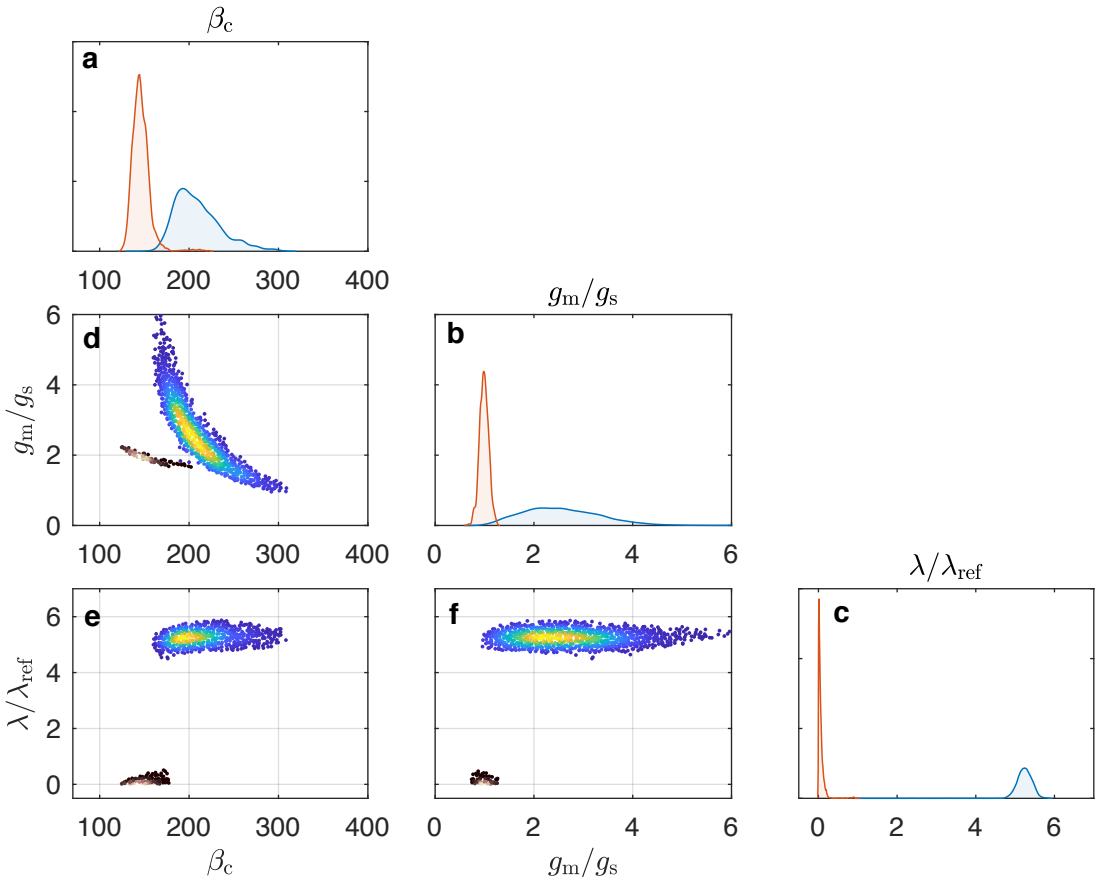


Figure 2: Probability distributions for three plant-specific parameters, estimated by MCMC for angiosperm (blue) and gymnosperm (red) species from global compilations of leaf and tree ring $\Delta^{13}C$ (correction "A"). (a) shows $\beta_c$, the ratio of carboxylation to transpiration cost factors); (b) shows $g_m/g_s$, the ratio of mesophyll to stomatal conductance; and (c) shows $\lambda/\lambda_{ref}$, which is the amount of $CO_2$ released from photorespiration per oxygenation reaction, relative to that of *N. tabacum* at 25$^o$C. All three parameters are unitless. (d-f) Two dimensional probability distributions showing covariance between parameters, estimated by MCMC.

### 4.2. *Simulations of plant $\Delta^{13}C$ over variable [$O_2$]:[$CO_2$] ratios*

Using our best-fit values for $\beta_c$, $g_m/g_s$, and $\lambda/\lambda_{ref}$, we simulated the expected responses of angiosperm and gymnosperm $\Delta^{13}C$ to [$CO_2$] from 200 to 1200 $\mu$mol mol$^{-1}$ (Fig. 3a), and [$O_2$]:[$CO_2$] ratios from ~200 to 1200 mol mol$^{-1}$ (Fig. 3b), both at 20$^o$C. The simulations show that gymnosperm $\Delta^{13}C$ does not change with [$O_2$] or [$CO_2$] levels, but decreases by $\sim$ 6 ‰ when $D$ is increased from 0.23 kPa (solid red lines, Fig. 3a) to 1.43 kPa (dashed red lines). For angiosperms, $\Delta^{13}C$ decreases strongly with lower [$CO_2$] at low $D$ (solid blue lines), but decreases slightly with lower [$CO_2$] at high $D$ (dashed blue lines). The $\Delta^{13}C$ offset between gymnosperms and angiosperms varies across [$CO_2$] levels.

For simplicity, we define the offset in discrimination between co-located (i.e same $T_d$ and $D$) angiosperm and gymnosperm plants as $\Delta^*_{a-g} = \Delta_a - \Delta_g$, where the subscripts "a" and "g" are adopted to indicate each plant group, respectively. The asterisk ($^*$) denotes an average isotopic offset between two tissues, rather than a fractionation in the strict sense. Figures 3b,c show that $\Delta^*_{a-g}$ decreases linearly with increasing [$O_2$]:[$CO_2$] ratio, when $T_d$ and $D$ are held constant. In addition, $\Delta^*_{a-g}$ values are greater at higher $D$ (dashed purple lines, Fig. 3c) and high $T_d$ (Fig. S3, see Electronic Annexure).

Because most ($> 70\%$) of the plants in our training dataset grew between $D = 0.23$ and $1.54$ kPa, Figure 3c shows that $\Delta^*_{a-g}$ is expected to fall in a large range between $+3.5$ and $-4.0$ ‰ at 20 $^o$C, over [$O_2$]:[$CO_2$] levels likely experienced over the Cenozoic (shaded purple region). The dependence of $\Delta^*_{a-g}$ on $T_d$ is weaker, and does not significantly affect this range, given the $T_d$ values in our dataset ($> 80\%$ between 17 and 23 $^o$C). The simulations show that the linear relationship between $\Delta^*_{a-g}$ and [$O_2$]:[$CO_2$] ratio is predominantly affected by the photorespiration term, rather than by the diffusion and carboxylation terms (Fig. 3c). Overall, at low $D = 0.23$ kPa, the photorespiration term contributes to up to $-9$‰ of the difference in $\Delta^{13}C$ between the two groups over the entire range of [$O_2$]:[$CO_2$] ratio, while the terms related to diffusion and Rubisco carboxylation account for $+4$‰ of $\Delta^*_{a-g}$ over this range.

### 4.3. *Dependence of $\Delta^*_{a-g}$ on D and atmospheric [$O_2$]:[$CO_2$] ratio: a semi-empirical linear model*

A semi-empirical expression can be derived for describing $\Delta^*_{a-g}$ in terms of both $D$ and [$O_2$]:[$CO_2$] ratios when plants from the two vascular groups are growing under the same environmental conditions:

$$\Delta^*_{a-g} \approx \varepsilon_f \frac{[O_2]}{[CO_2]} + \varepsilon_{ab} D + \varepsilon_0 \tag{8}$$

where $\varepsilon_f$ is a coefficient related to the difference in fractionation between angiosperms and gymnosperms due to photorespiration terms, and $\varepsilon_{ab}$ is a coefficient related to differences attributed to $CO_2$ diffusion and carboxylation. At this stage the meaning of the third term, $\varepsilon_0$ is not fully clear, but is included to describe all other remaining contributions (including differences in respiration, random effects, etc.), which we assume to be constant. Because the $CO_2$ compensation point is related to $\lambda$, the chloroplastic oxygen concentration $O_c$ (in turn related to [$O_2$]) and

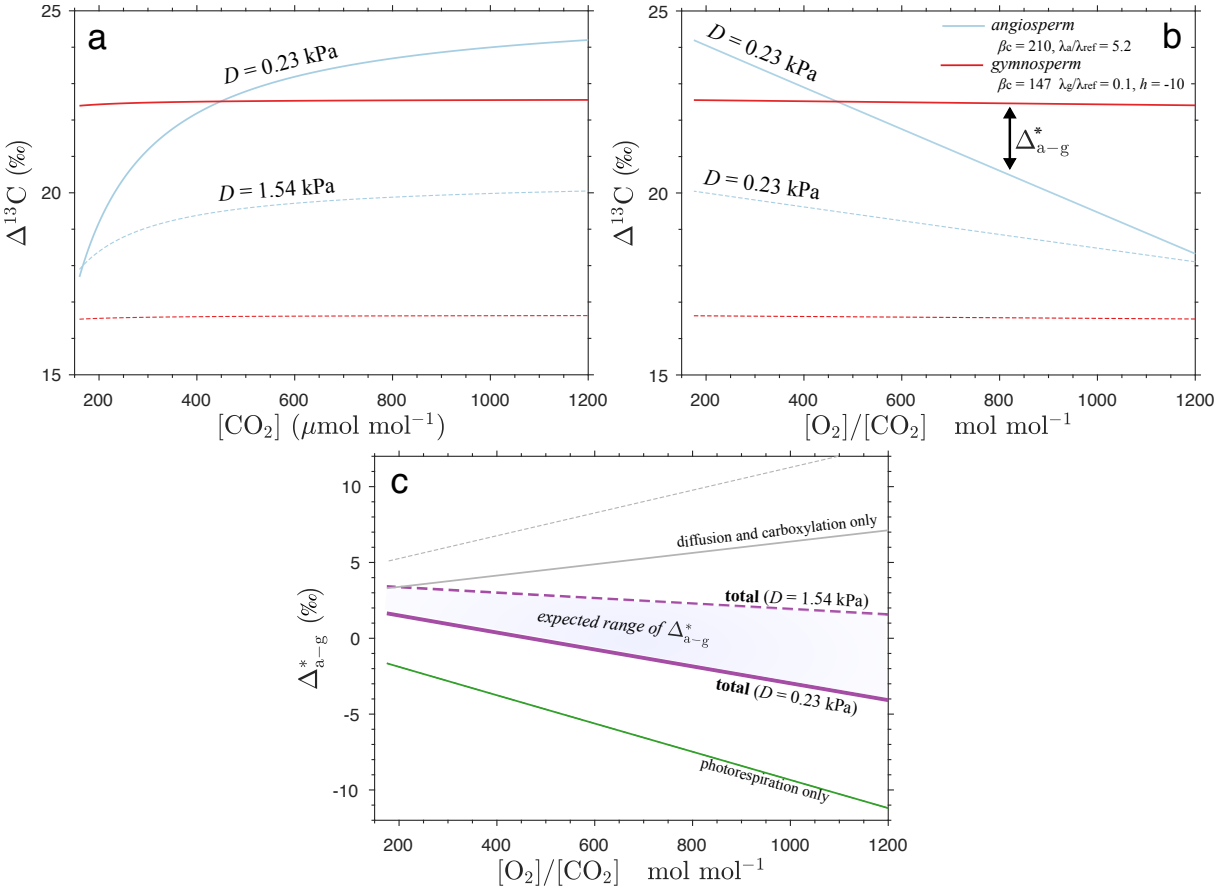


Figure 3: Simulations of the effects of $[O_2]$:$[CO_2]$ ratio on plant $\Delta^{13}C$ for different environmental conditions. We used the best-fit values for plant specific traits ($\beta_c$, ratio of carboxylation to transpiration cost factors; $g_m/g_s$, ratio of mesophyll to stomatal conductances; and $\lambda$, the amount of $CO_2$ released by photorespiration per oxygenation reaction) as estimated from the MCMC approach applied to Eqns. (5-7). Parameters are listed in Table (2). (a) shows the effect of atmospheric $CO_2$ concentrations on $\Delta^{13}C$ for angiosperms (blue curves) and gymnosperms (red), both at vapour pressure deficits of $D = 1.54$ kPa (dashed lines) and $D = 0.23$ kPa (solid lines); (b) shows the corresponding curves plotted against $[O_2]$:$[CO_2]$ ratio, and (c) $\Delta^*_{a-g} = \Delta_a - \Delta_g$ against $[O_2]/[CO_2]$ (purple curves), along with contributions from each term separately (green and grey lines).

the Rubisco specificity, $S_{c/o}$ (Busch, 2020), the first term can be approximated (using Eqns. 4-5) as:

$$\varepsilon_f \approx S_{c/o}^{-1}\left[\lambda_g(f - wh_g) - \lambda_a(f - wh_a)\right] \tag{9}$$

where the subscripts a and g denote angiosperm and gymnosperm-specific $\lambda$ values, respectively. Eqns. (8-9) provide a simple, but powerful framework for interpreting co-located plant isotope records. Eqn. 8 predicts that $\Delta^*_{a-g}$ will vary linearly with both $D$ and $[O_2]/[CO_2]$, if $\varepsilon_{ab}$ and $\varepsilon_f$ are constant. Eqn. 9 predicts the slope of $\Delta^*_{a-g}$ versus $[O_2]/[CO_2]$ will be negative if $\lambda_a > \lambda_g$, and will be steeper if differences in $\lambda$ increase. It is possible that $\lambda$ may vary in a subtle way from species to species within each plant group, although this is yet to be determined. Such variations might lead to slightly different $\varepsilon_f$ when comparing a single species of gymnosperm to another species of angiosperm at any given location. However, when several species are compared, we expect this variation will be averaged out, because according to our analysis, differences in $\lambda$ appear to be fairly robust across each plant group.

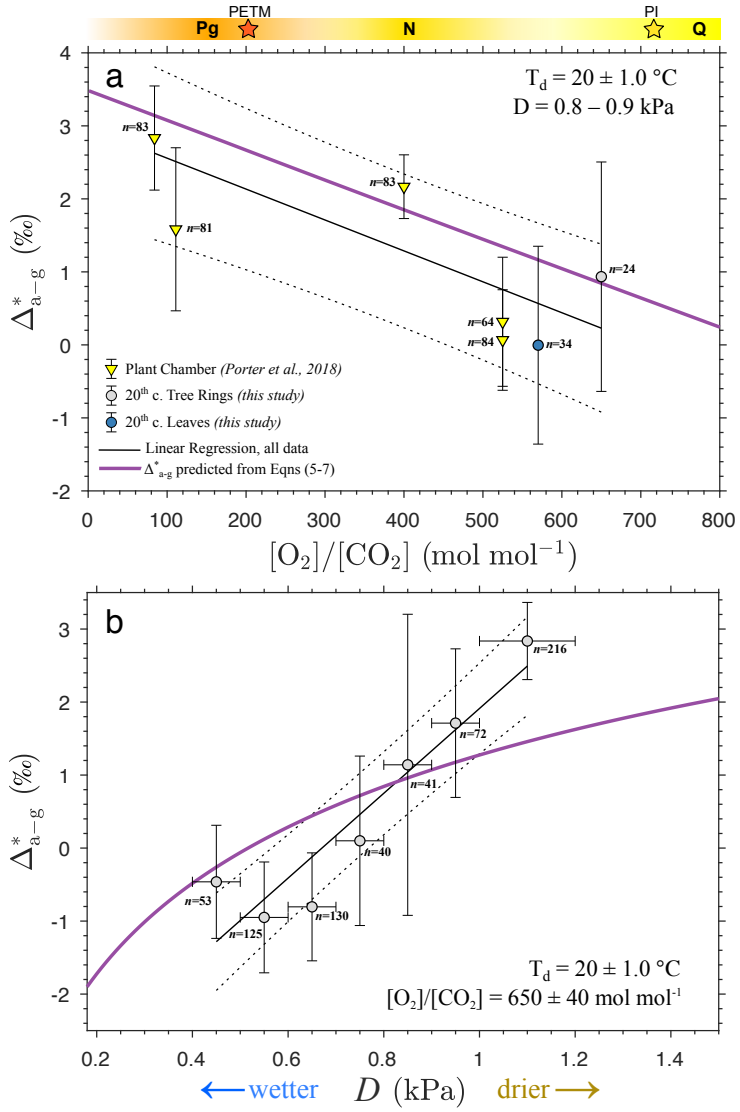


Figure 4: Differences between average angiosperm and gymnosperm carbon isotope discrimination, $\Delta^*_{a-g}$, inferred from plant chamber, leaves and tree ring data at 20 $^o$C, (a) plotted against $[O_2]/[CO_2]$ at vapor pressure deficit ($D$) of 0.85 kPa, and (b) against vapor pressure deficit at $[O_2]/[CO_2]$ = 650 mol mol$^{-1}$. The bars represent the 95% confidence intervals of the $\Delta^*_{a-g}$ values. (a) shows linear partial least-squares fit in black over a range of $[O_2]/[CO_2]$ from 400-650 mol mol$^{-1}$, with 1$\sigma$ prediction bounds. Errors in $[O_2]/[CO_2]$ are approximately the size of each datapoint. In (b), a partial linear least-squares fit is shown in black over 0.45 to 1.1 kPa, error bars indicating the bin width, with the total number ($n$) of angiosperm and gymnosperm data within each bin indicated next to each datapoint.The fitted coefficients are $\varepsilon_f = -0.004 \pm 0.002$ ‰ mol mol$^{-1}$, $\varepsilon_{ab} = 5.9 \pm 1.3$ ‰ mol mol$^{-1}$ (1$\sigma$), and $\varepsilon_0 = -0.9$ ‰ (Eqn. 8). The relationship predicted according to the comprehensive *ab initio* model (Eqns 5-7) is also shown in heavy purple lines. For comparison, a rough timescale for the Cenozoic is shown at the top of the figure (note: it is likely that there was considerable overlap in the $[O_2]$:$[CO_2]$ range of the Palaeogene and Neogene). PI = pre-industrial value, Q = Quaternary, N = Neogene, Pg = Paleogene, PETM = Paleocene-Eocene Thermal Maximum.

Our proposed model (Eqn. 8) is simple enough to be tested against stable carbon isotope data from plant chamber experiments, as well as tree rings and leaves (see Fig. 4a,c caption, and details of "testing dataset" in Methods). Overall, $\Delta^*_{a-g}$ shows significant variation with both $D$ (Fig. 4b) and $[O_2]/[CO_2]$ (Fig. 4a). $\Delta^*_{a-g}$ decreases with $[O_2]/[CO_2]$ modestly, from approximately 100 to 650 mol mol$^{-1}$ (Fig. 4a), as would be expected from our linear model (Eqn. 8). The linear fit to the data over the 100–650 mol mol$^{-1}$ range of $[O_2]/[CO_2]$ values yields a slope of

$\varepsilon_f = -0.004 \pm 0.002$ ‰ mol mol$^{-1}$ ($1\sigma$), with an intercept of $3.0 \pm 1.0$ ‰. Although there is more scatter in this relationship (adjusted $R^2$ = 0.51) and the trend is modest, it is in agreement with the slope predicted by Eqns. (5-7) to within $1\sigma$ prediction bounds. Note that to ensure robust binning, a minimum number of 6 angiosperms and 6 gymnosperm $\Delta^{13}$C values were used in the calculation of $\Delta^*_{\mathrm{a-g}}$. Fits are found to be somewhat insensitive to the binning procedure when a different bin width (i.e., 30 mol mol$^{-1}$) is chosen; the resulting regressed coefficients are not significantly different ($\varepsilon_f = -0.0037 \pm 0.0014$ ‰ mol mol$^{-1}$). All binned data can be found in the Electronic Annexure.

The slope of $\Delta^*_{\mathrm{a-g}}$ versus $D$ is higher than that of $\Delta^*_{\mathrm{a-g}}$ versus [$O_2$]/[$CO_2$], and in the opposite direction (Fig. 4b). A linear fit to the binned data in Figure 4b yielded a positive slope of $\varepsilon_{ab} = 5.9 \pm 1.3$ ‰ mol mol$^{-1}$ ($1\sigma$), with an intercept of $-3.9 \pm 1.0$ (adjusted $R^2 = 0.86$). This result is in general agreement with the predictions (purple lines, Fig. 4b) at moderate $D$ levels (i.e. between 0.7 and 1 kPa). However, the slope of $\Delta^*_{\mathrm{a-g}}$ versus $D$ as implied by the data, is greater than that predicted by Eqns. (5-7). Figure 4b shows that the predictions using Eqns. (5-7) diverge slightly from the trend in the data at $0.5 < D < 0.7$ kPa and at $> 1$ kPa.

Finally, using our fitted value for $\varepsilon_f$, it is possible to calculate the Rubisco specificity ($S_{\mathrm{c/o}}$) using Eqn. 9. We estimated that $S_{\mathrm{c/o}} = 290$ mol mol$^{-1}$, assuming $f = 11$‰ , $h_{\mathrm{a}} = -1$‰, $h_{\mathrm{g}} = -10$‰, $\lambda_{\mathrm{ref}} = 0.6$, and using the previously-estimated values for $\lambda_{\mathrm{a}}/\lambda_{\mathrm{ref}}$, and $\lambda_{\mathrm{g}}/\lambda_{\mathrm{ref}}$ (i.e., 5.2 and 0.1, respectively, Section 4.1), as well as the solubility conversion factors (liquid to gas phase) from Galmés et al. (2016).

## 5. Discussion

### *5.1. Basis for the relationships between $\Delta^*_{\mathrm{a-g}}$, D, and [$O_2$]/[$CO_2$]*

The relationships between $\Delta^*_{\mathrm{a-g}}$ and vapor pressure deficit ($D$), and between $\Delta^*_{\mathrm{a-g}}$ and [$O_2$]/[$CO_2$], at least over 100 to 650 mol mol$^{-1}$, are both noteworthy. To the best of our knowledge, none of them has been described before - but both follow from the comprehensive *ab initio* model of discrimination (see Sections 2 and 4.2), and from key differences in plant-specific traits. These traits are: $\beta_{\mathrm{c}}$, the ratio of cost factors for carboxylation and transpiration ; $g_{\mathrm{m}}/g_{\mathrm{s}}$, the ratio of mesophyll to stomatal conductances for $CO_2$; and $\lambda/\lambda_{\mathrm{ref}}$, the parameter related to photorespiration (Section 4.1). Gymnosperm $\Delta^{13}$C is more sensitive to $D$ than angiosperms. This is because lower values of $g_{\mathrm{m}}/g_{\mathrm{s}}$ in gymnosperms amplify the response of $\chi_{\mathrm{c}}$ to $D$, via Eqn. (6). In addition, gymnosperms are less responsive to [$CO_2$] because $\lambda/\lambda_{\mathrm{ref}}$ is generally much lower in this plant group than in angiosperms, reducing the photorespiratory compensation point (Eqn. 4). Our findings therefore support the recent study of Sheldon et al. (2020), who found that gymnosperm $\Delta^{13}$C values obtained from herbarium records were largely insensitive to rising levels of [$CO_2$] from 1850 CE to present - and provide a mechanistic explanation for these authors' observations.

Rubisco specificity is fairly well constrained in $C_3$ plants, with a range of around 85-110 mol mol$^{-1}$ at 25 $^o$C, with little variation according to $C_3$ phylogenetic group (Orr et al., 2016). Using a compilation of *in vitro* data, as well as leaf data, Galmés et al. (2016) obtained an average value of 108 mol mol$^{-1}$ at 20$^o$C. Our value of 290 mol mol$^{-1}$ is thus higher than the range of values obtained in the literature, although relatively of the same order of magnitude.

It is worth noting that a rough estimate of the Rubisco specificity - a fundamental parameter in the biochemistry of photosynthesis - can be obtained independently from carbon isotopic measurements at known $[O_2]/[CO_2]$ levels using a simple linear fit. It gives us confidence in the generality of our findings. One possible explanation for our higher than average estimate might be inaccuracies in the (assumed) values of $\lambda_{\mathrm{ref}}$ and $h$. For instance, a value of 0.2 for $\lambda_{\mathrm{ref}}$ would decrease our estimate of $S_{\mathrm{c/o}}$ to 97 mol mol$^{-1}$, which would be more consistent with values from the literature. We expect that it will be possible to better constrain $S_{\mathrm{c/o}}$ once further information about $\lambda_{\mathrm{ref}}$ and $h$ become available.

How can the variation in $\lambda/\lambda_{ref}$ be interpreted? There is currently no published study investigating the values for $\lambda$, but we can get insights from the theory. Busch (2020) define the variable as $\lambda = 0.5(1-\alpha_{\mathrm{G}})+\alpha_{\mathrm{T}}$, where $\alpha_{\mathrm{G}}$ is the proportion of glycine removed from the photorespiratory pathway, and $\alpha_{\mathrm{T}}$ is proportion of 2-phosphoglycolate carbon exported as $CH_2$-THF. Glycine is produced via the photorespiratory pathway, and forms a key precursor of compounds (e.g. dehydrins, glycine betaine) which are accumulated in higher plants in response to environmental stresses such as dessication and damage by reactive oxygen radicals, e.g. Sakamoto and Murata (2002). We suggest that higher $\alpha_{\mathrm{G}}$ values in gymnosperms (hence lower $\lambda$) is consistent both with ecology (e.g. conifer tolerance to drought), as well as gymnosperm evolutionary history (evolution under high $[O_2]$ atmospheres). The effects of $\lambda/\lambda_{\mathrm{ref}}$ on $\Delta^{13}\mathrm{C}$ also underscore the importance of incorporating photorespiration into models of $C_3$ plant discrimination, which has been suggested by other studies (Schubert and Jahren, 2018; Zhang et al., 2019; Lavergne et al., 2019). We note that the value of $h = -10$ ‰, found in our study for gymnosperms, is consistent with the analysis of Schubert and Jahren (2018). According to our analysis, and Eqn. (3), the term $f - wh$ behaves as an apparent fractionation with large combined magnitude of $\sim$ 21 ‰, which is close to the best-fit value of $f$ proposed by Schubert and Jahren (2018) of 19.2 ‰, without considering $h$.

Our results also imply that our values for $\lambda$ are higher than tobacco ($\lambda_{\mathrm{ref}}$). This could be interpreted as higher proportion of $CH_2$-THF exported for lignin production, because our compilation is almost entirely from trees (as opposed to lab-grown herbaceous plants). Walker et al. (2017) suggested $\lambda_{\mathrm{ref}} = 0.6$ at 25$^o$C for tobacco, and identified a positive relationship between $\lambda$ and temperature. However, these relationships are still speculative, and so robust quantification of the true value of $\lambda$ is not currently possible using our dataset. Regardless of the true values of $\lambda$ or $\lambda_{\mathrm{ref}}$, differences between $\lambda/\lambda_{\mathrm{ref}}$ for our gymnosperm and angiosperm records appear to be robust, and offer a convincing explanation for group-specific responses to changes in atmospheric $[CO_2]$ in tree ring studies (e.g. Voelker et al. (2016)) and faunal collagen (Hare et al., 2018), and to changes in $[O_2]$ levels (Porter et al., 2017).

### *5.2. Implications for Cenozoic records of stable carbon isotopes*

Although previous geological studies (e.g. Diefendorf et al. (2015); Bechtel et al. (2019); Schlanser et al. (2020a)) have assumed a constant offset of 2-3 ‰ between co-located angiosperm and gymnosperm $\Delta^{13}\mathrm{C}$ plants, our results suggest that this offset (i.e., $\Delta^{*}_{\mathrm{a-g}}$) is variable over geological timescales. Our empirical linear model for $\Delta^{*}_{\mathrm{a-g}}$ (Eqns. 8-9) is directly applicable to the terrestrial geological record, assuming that the fossil plant materials considered for gymnosperms and angiosperms came from the same area, and plants originally grew under similar

environmental conditions. In these cases, $\Delta^*_{a-g}$ should increase at higher $D$ and atmospheric [$CO_2$] (assuming constant [$O_2$]). According to our fits (Fig. 4), these relationships should hold for many levels of $D$, [$O_2$] and [$CO_2$] over the Cenozoic, although more data are needed to evaluate whether it holds at much higher [$O_2$]/[$CO_2$], i.e. LGM to pre-Industrial conditions of $> 700$ mol mol$^{-1}$. No published data are yet available for testing this hypothesis, but it would be a good test of the framework, because $\Delta^*_{a-g}$ should be negative during the LGM, when [$O_2$]/[$CO_2$] was very high, and $D$ was generally lower.

$\Delta^*_{a-g}$ values calculated from Cenozoic paleo-data generally support our novel interpretation. Figure 5 shows that $\Delta^*_{a-g}$ values were very high (around $+4$ ‰ and higher) during the Palaeocene-Eocene ($\sim$ 63 – 52 Ma), when [$CO_2$] was high, but decreased to around $+2.5$ ‰ in the Miocene (Bechtel et al., 2019, 2008), when [$CO_2$] was lower. The lowest $\Delta^*_{a-g}$ values ($-2$ ‰) are observed in the $20^{th}$ century from leaves and tree rings records when [$CO_2$] and/or $D$ levels were lower. In this figure, the observed $\Delta^*_{a-g}$ values are plotted against those predicted from the comprehensive model (Eqn. 5-7), using the palaeo-[$CO_2$] curve of Foster et al. (2017), and assuming [$CO_2$] equal to $\sim$1010 $\mu$mol mol$^{-1}$ over the PETM according to Gehler et al. (2016). Note that it is difficult to estimate the corresponding growing-season $D$ and $T_d$ values for paleo-data, but for simplicity, we have chosen nominal values of 0.8 kPa and 20$^o$C. These values describing a relatively moist atmosphere are consistent with moderate to high levels of moisture availability as reconstructed from paleobotanical data for the Paleocene-Eocene (Eberle and Greenwood, 2012; Greenwood et al., 2010; West et al., 2015) and Miocene (Bechtel et al., 2019) sites.

Figure 5 also shows trends in modern tree ring data. In an extensive survey, Leavitt and Newberry (1992) found that average differences in identical-age rings from Wisconsin formed in 1992 CE (green squares) decreased with site latitude across a gradient from 41$^o$N (average $D = 1.3$ kPa) to 45.5$^o$N (average $D = 0.8$ kPa). These trends are also consistent with our model, which predicts that $\Delta^*_{a-g}$ must decrease with increasing site latitude, because $D$ decreases.

Our results show a slight deviation from the 1:1 line. The *ab initio* model based on Eqns. (5-7) generally underestimates the high $\Delta^*_{a-g}$ values and overestimates the low values - but the observed and predicted $\Delta^*_{a-g}$ values are in relatively good agreement across different tissues (tree rings cellulose/lipid), time periods, and angiosperm and gymnosperm species ($R^2$ = 0.509, RMSE = 0.538, $p$-value $< 0.001$). The slight deviation of predicted values from the observations might be due to systematic biases in the paleo-data or issues with some of the model assumptions. Further work using a larger observational dataset, particularly derived from plant chamber experiments, will very likely contribute to improve the predictive skills of the model.

It is worth noting that other factors not accounted for in our framework could potentially modulate $\Delta^*_{a-g}$ variations in the geological record. For instance, it is possible that some of the range in $\Delta^*_{a-g}$ values, particularly in the case of lipid data, could be explained by group-specific post-photosynthetic fractionations. In Figure 5 we corrected fossil $\delta^{13}$C data for post-photosynthetic fractionations following Diefendorf et al. (2012), i.e., using constant values of $\varepsilon_{lipid} = -0.4$ ‰ and $\varepsilon_{lipid} = -0.6$ ‰ for angiosperm and gymnosperm terpenoids, respectively. However, a recent study has shown that $\varepsilon_{lipid}$ values vary substantially between different gymnosperm clades (Diefendorf

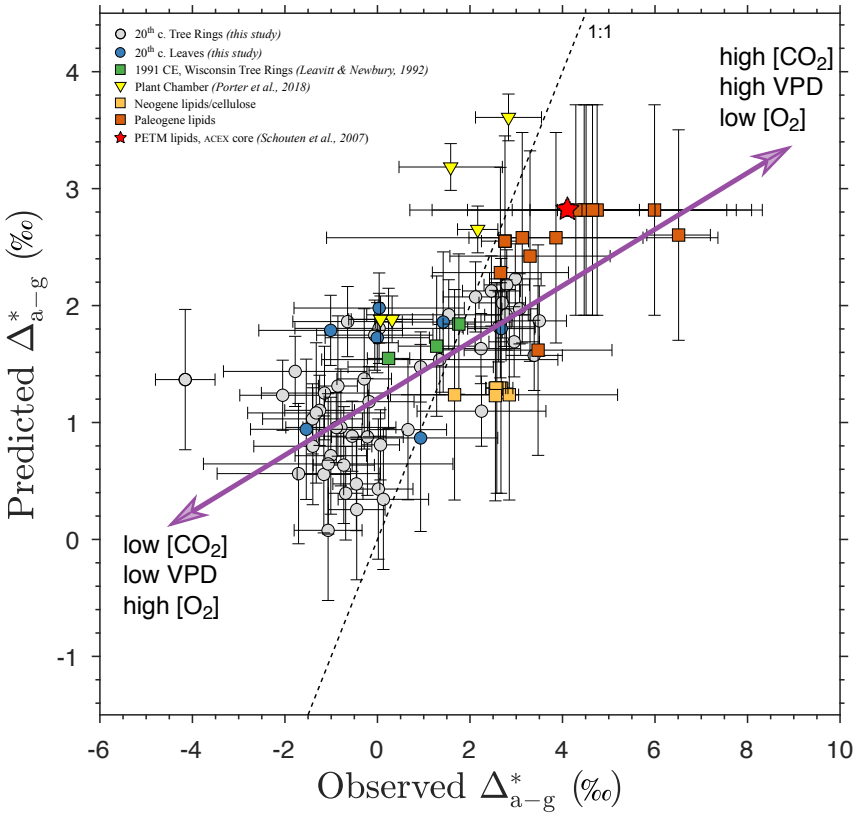


Figure 5: Changes in $\Delta^*_{a-g}$ across the Cenozoic, predicted from Eqns. (5-7), versus observed values, including $20^{th}$ century tree ring and leaf data (grey and blue circles), tree ring data from Leavitt and Newberry (1992) (green squares), and plant chamber experiments (Porter et al., 2017) (yellow triangles). Errorbars are 95% CI. Paleogene lipid data: Bighorn Basin, Wyoming (Diefendorf et al., 2015), Canadian Arctic, and Driftwood Canyon, British Colombia (Schlanser et al., 2020a), ACEX core, Arctic Schouten et al. (2007). Neogene lipid and cellulose data: Poland and Austria Bechtel et al. (2008, 2019). Lipid data are corrected for variations in post-photosynthetic fractionations between angiosperms and gymnosperms (e.g. $\varepsilon_{\text{lipid}} = -0.4$ ‰ and $\varepsilon_{\text{lipid}} = -0.6$ ‰ for angiosperm and gymnosperm terpenoids (Diefendorf et al., 2012), respectively). PETM: Paleocene-Eocene Thermal Maximum.

et al., 2019). This variation is expected to be averaged if several species of gymnosperms grew together, but it is difficult to know the size of the effect on $\Delta^*_{a-g}$ if the isotopic record considered is biased towards one particular species. There are other potentially confounding effects on geological $\Delta^*_{a-g}$ values. Older leaves tend to be more depleted in $^{13}$C than younger leaves, by up to 2.1 ‰ (Vogado et al., 2020), because $^{13}$C-depleted photosynthetic carbon is used along with carbon imported from outside the leaf as the leaf develops. This might lead to age-related difference in $\Delta^{13}$C between plant species that retain their leaves for long times (e.g. evergreens) and deciduous plants. Further research is needed to better understand and quantify these effects on $\Delta^*_{a-g}$.

### *5.3. Implications for paleo-[$CO_2$] proxies based on $C_3$ plant discrimination*

Two models of carbon isotope discrimination are currently used to estimate paleo-[$CO_2$] from fossil $C_3$ plant matter (Schubert and Jahren, 2012; Franks et al., 2014), and both models have been extensively applied to Cenozoic records (Cui and Schubert, 2018; Cui et al., 2020; Reichgelt et al., 2020; Royer et al., 2019). Both formulations are related to the FvCB model (Schubert and Jahren, 2018; Hollis et al., 2019) but differ according to their parameterisation and assumptions. In the Franks et al. (2014) model, phylogenic dependencies are incorporated via a term for

the maximum total conductance of $CO_2$ ($g_{s,max}/1.6$) obtained from measurements of stomatal size and density, and photorespiration is assumed to be negligible. In the Schubert and Jahren (2018) model (see also Schubert and Jahren (2012)), discrimination is assumed to be largely independent of phylogeny (with constant $\Delta^*_{a-g}$), but photorespiration terms are effectively included (i.e. the hyperbolic relationship in this model is functionally equivalent to Eqn. (5) but assuming constant $\Gamma^*$). Presently, there is no easy way to include a term for atmospheric humidity (i.e. $D$, indirectly related to soil moisture availability), [$O_2$], or variable $\Gamma^*$, explicitly in either model. All of these effects could lead to biases in palaeo-[$CO_2$] estimated from fossil $C_3$ plant matter, if unaccounted for (Hollis et al., 2019). Porter et al. (2019) recently suggested that these paleo-[$CO_2$] proxies could be further improved by correcting for the effects of [$O_2$] and phylogeny, while Steinthorsdottir et al. (2020) recently showed that better precision and accuracy can sometimes be achieved if several angiosperm and gymnosperm species from one location are used, rather than individual species. These suggestions are consistent with our approach and give us confidence about the relevance of our findings.

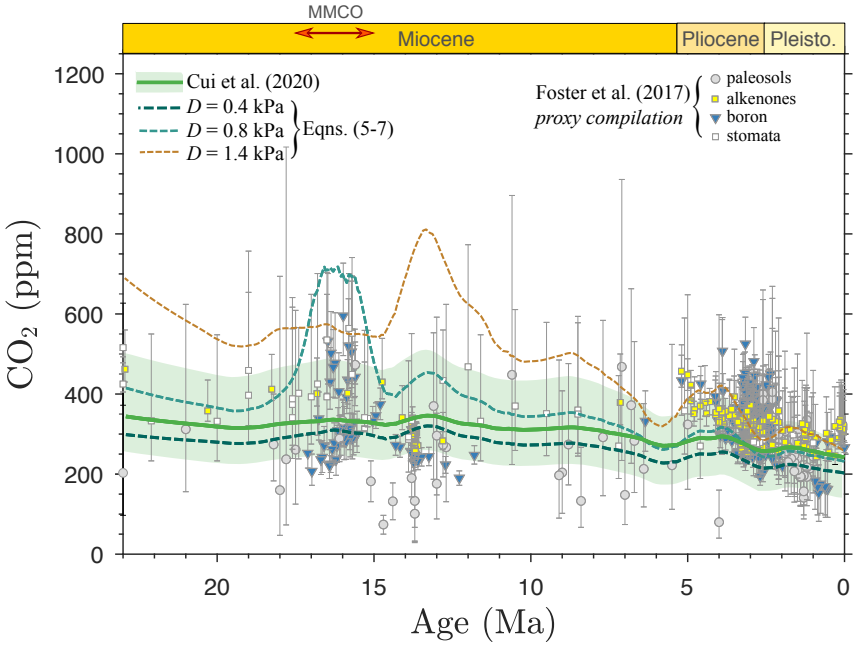


Figure 6: Paleo-[$CO_2$] proxies across the Cenozoic, showing the recent curve of Cui et al. (2020), based on the model of $C_3$ land plant discrimination of Schubert and Jahren (2012, 2018) (heavy green line, with shaded green area representing 84% confidence intervals from Cui et al. (2020)). Dashed green lines represent paleo-[$CO_2$] estimated by numerical solution of Eqns. (5-7), this study, applied to the same data compilation of Cui et al. (2020), with locally weighted (LOWESS, $\alpha$=0.15) fits through $n = 461$ data points (not shown), at three different levels of vapor pressure deficit ($D = 0.4, 0.8, 1.4$ kPa). For numerical modeling, best-fit parameters for angiosperms (Section 4.1, this study) were used. For comparison, raw paleo-[$CO_2$] proxy data from the compilation of Foster et al. (2017) is also shown (see references therein for paleosol, alkenone, boron, and stomatal datasets). Pleisto: Pleistocene; MMCO: Mid-Miocene Climatic Optimum.

Overall, our results suggest that all the above-mentioned factors - photorespiration, [$O_2$], phylogentic dependence, and variable $\Gamma^*$ - are important to include in paleo-[$CO_2$] proxies based on discrimination in terrestrial $C_3$ plants. Although further investigations are necessary (but are beyond the scope of this study), the framework presented here should provide a way forward to correct paleo-[$CO_2$] proxies for these effects. To illustrate this point, we consider the recent record of palaeo-[$CO_2$] from Cui et al. (2020) dominated by angiosperm plants growing in sites with

relatively high atmospheric humidity (low $D$). In Figure 6 we compare the respective paleo-[$CO_2$] data points with those predicted from Eqns (5-7) (numerical solution estimated using the MATLAB 'solve' function) using the Cui et al. (2020) dataset and the best-fit values from our Table 2 for angiosperms. The resulting paleo-[$CO_2$] predicted by this method (dashed curves in Fig. 6) agrees with the curve of Cui et al. (2020) at low $D$ levels ($D = 0.4$ kPa, dashed heavy teal line), to within uncertainties. In this figure, we also plot palaeo-[$CO_2$] data derived from the compilation of Foster et al. (2017). Our curve at $D = 0.4$ kPa also agrees with the spline of Foster et al. (2017) (for clarity, not shown) to within uncertainties. We note that the agreement with Cui et al. (2020) at low $D$ is perhaps unsurprising, considering that the Schubert and Jahren (2018) model is biased towards chamber data, with low $D$ levels.

However, our [$CO_2$] curves at higher $D$ levels (i.e., $D = 0.8$ and $D = 1.4$ kPa, dashed blue and brown lines) are significantly higher than the curve of Cui et al. (2020). Considering that fewer than 10% of trees in our modern global compilation grew at $D < 0.4$ kPa, and over 50% of angiosperms grew at $D > 1.0$ kPa, higher $D$ levels are possible in the fossil record. If $C_3$ plants originally grew under higher $D$ levels, then our estimates at $D = 0.8$ and $D = 1.4$ kPa would result in [$CO_2$] values ranging between 550 and 700 ppm at the Mid-Miocene Climatic Optimum (MMCO, 17 to 15 Ma ago).

Steinthorsdottir et al. (2020) recently estimated paleo-[$CO_2$] from MMCO Lagerstätte deposits using different approaches; i.e., 402 - 614 ppm using stomatal methods, 364 - 609 ppm using the Franks et al. (2014) method, and 471 - 624 ppm using the $C_3$ proxy method of Schubert and Jahren (2012). Their estimates are higher than previously inferred from carbonate and $\delta^{11}B$ (400 - 450 ppm; Foster et al. (2017)). [$CO_2$] values around 400 - 450 ppm as suggested by the last study imply extremely high equilibrium climate sensitivity (ECS), i.e. warming of 5 $^oK$ at the MCO for a doubling of [$CO_2$], which is out of the 2.3 - 4.7 $^oK$ range proposed by a growing number of studies based on both modern and paleo-records (e.g., Sherwood et al. (2020)). The range of [$CO_2$] values implied by our re-modeling of the Cui et al. (2020) compilation, and by Steinthorsdottir et al. (2020) are more consistent with an ECS lower than 5 $^oK$, suggesting that [$CO_2$] should be revised upwards for the MCO in paleo reconstructions.

Although incorporating greater diversity of plant physiological responses (Porter et al., 2019; Yiotis and McElwain, 2019; Steinthorsdottir et al., 2020), and/or increasing the number of parameters into models (Konrad et al., 2020) might help to improve the accuracy of paleo-[$CO_2$] proxies, there are nevertheless disadvantages to our approach. For instance, our proposed framework assumes constant anatomical and physiological differences across plant evolutionary history (particularly with respect to photorespiration), or even within a single plant lifetime, which might not be the case (Reich et al., 2018). Nevertheless, the differences identified here are robust across a wide variety of woody species, and environments. Further research is needed to determine whether these relationships hold over a wider range of temperatures, [$O_2$]:[$CO_2$] ratios, water availability, and nutrient regimes.

## 6. Conclusion

In this study, we aimed to better understand the factors that influence differences in $\Delta^{13}\mathrm{C}$ between angiosperm and gymnosperm $C_3$ woody plants. Using a comprehensive *ab initio* model of carbon isotope discrimination, and training it against a very large $20^{th}$ century dataset, we demonstrated that isotope discrimination is phylogeny-dependent. Multiple intrinsic physiological factors give rise to differences in gymnosperm and angiosperm $\Delta^{13}\mathrm{C}$ values - including $\beta_\mathrm{c}$ - the ratio of cost factors for carboxylation to transpiration (related to leaf physiology), $g_\mathrm{m}/g_\mathrm{s}$ - the ratio of mesophyll to stomatal conductances for $CO_2$ (related to leaf morphology), and $\lambda$ - the fraction of $CO_2$ released during photorespiration (related to plant carbon metabolism).

We also showed that the $\Delta^{13}\mathrm{C}$ offset between the two $C_3$ plant groups is very likely not constant over time, but varies with environmental conditions, and changes in atmospheric $[O_2]$:$[CO_2]$ ratio. Overall, our results can be summarised as follows:

- $\Delta^{13}\mathrm{C}$ in angiosperms is more sensitive to $[CO_2]$ than in gymnosperms;
- $\Delta^{13}\mathrm{C}$ in gymnosperms is more sensitive to $D$ than in angiosperms;
- $\Delta^*_{\mathrm{a-g}}$ increases modestly with decreasing $[O_2]$:$[CO_2]$ ratio, and/or increasing $[CO_2]$,
- $\Delta^*_{\mathrm{a-g}}$ increases strongly with increasing $D$.

These findings have important implications for geological studies because they suggest that the substantial variations of stable carbon isotopic composition observed in the geological record (up to 7 ‰) reflect not only diagenesis, or post-photosynthetic fractionation (as has been previously assumed), but also different plant responses to $D$, and changing atmospheric $[O_2]$:$[CO_2]$ ratios. On the other hand, the simple model presented here for $\Delta^*_{\mathrm{a-g}}$ (Eqn. 8) presents an opportunity to refine $\Delta^{13}\mathrm{C}$-based proxies of paleoatmospheric composition, if diagenesis can be ruled out, and $D$ levels can be independently constrained.

Our framework reconciles previously unexplained observed patterns, such as covariation of modern tree ring $\Delta^*_{\mathrm{a-g}}$ with latitude (and $D$) (Leavitt and Newberry, 1992), variable $[O_2]$ (Porter et al., 2017), and differences during glacial maxima (Hare et al., 2018; Breecker, 2017). It also offers a testable relationship that can be evaluated and refined using plant chamber experiments and field observations. For instance, we predict that $\Delta^*_{\mathrm{a-g}}$ will increase in future decades of the $21^{st}$ century, because $D$ is likely to rise along with anthropogenic $[CO_2]$ emissions.

*Declaration of Competing Interest*

The authors declare that they have no known competing financial interests or personal relationships that could have appeared to influence the work reported in this paper.

## Acknowledgments

This work was supported by a South African NRF - ERC Partnership Grant (No. 120141) to VJH for research leave to Imperial College, kindly hosted by H. Graven. A.L. was supported by a Marie Sklodowska-Curie Individual

Fellowship under the European Union's Horizon 2020 Research and Innovation Programme (Grant agreement no: 838739 ECAW-ISO). We thank S. Leavitt, I. C. Prentice, and Caitlyn Witkowski, for helpful suggestions, and comments. The meticulous and constructive comments of three anonymous reviewers are appreciated.

## References

Bechtel A., Gratzer R., Sachsenhofer R. F., Gusterhuber J., Lücke A. and Püttmann W. (2008) Biomarker and carbon isotope variation in coal and fossil wood of Central Europe through the Cenozoic. *Palaeogeography, Palaeoclimatology, Palaeoecology* **262**(3-4), 166–175.

Bechtel A., Widera M. and Woszczyk M. (2019) Composition of lipids from the First Lusatian lignite seam of the Konin Basin (Poland): Relationships with vegetation, climate and carbon cycling during the mid-Miocene Climatic Optimum. *Organic Geochemistry* **138**, 103908.

Bereiter B., Eggleston S., Schmitt J., Nehrbass-Ahles C., Stocker T. F., Fischer H., Kipfstuhl S. and Chappellaz J. (2015) Revision of the EPICA Dome C CO2 record from 800 to 600 kyr before present. *Geophysical Research Letters* **42**(2), 542–549.

Bernacchi C. J., Portis A. R., Nakano H., von Caemmerer S. and Long S. P. (2002) Temperature response of mesophyll conductance. Implications for the determination of Rubisco enzyme kinetics and for limitations to photosynthesis in vivo. *Plant physiology* **130**(4), 1992–1998.

Breecker D. O. (2017) Atmospheric $pCO_2$ control on speleothem stable carbon isotope compositions. *Earth and Planetary Science Letters* **458**, 58–68.

Busch F. A. (2020) Photorespiration in the context of Rubisco biochemistry, CO2 diffusion, and metabolism. *The Plant Journal* **101**, 919–939.

Busch F. A., Holloway-Phillips M., Stuart-Williams H. and Farquhar G. D. (2020) Revisiting carbon isotope discrimination in C3 plants shows respiration rules when photosynthesis is low. *Nature Plants* **6**(3), 245–258.

Busch F. A., Sage R. F. and Farquhar G. D. (2018) Plants increase CO2 uptake by assimilating nitrogen via the photorespiratory pathway. *Nature plants* **4**(1), 46.

Cernusak L. A., Tcherkez G., Keitel C., Cornwell W. K., Santiago L. S., Knohl A., Barbour M. M., Williams D. G., Reich P. B., Ellsworth D. S. *et al.* (2009) Why are non-photosynthetic tissues generally 13C enriched compared with leaves in C3 plants? Review and synthesis of current hypotheses. *Functional Plant Biology* **36**(3), 199–213.

Cornwell W. K., Wright I., Turner J., Maire V., Barbour M., Cernusak L., Dawson T., Ellsworth D., Farquhar G., Griffiths H. *et al.* (2016) A global dataset of leaf delta 13C values. *Scientific Data* .

Craig H. (1954) Carbon 13 in plants and the relationships between carbon 13 and carbon 14 variations in nature. *The journal of geology* pp. 115–149.

Cui Y. and Schubert B. A. (2018) Towards determination of the source and magnitude of atmospheric pCO2 change across the early Paleogene hyperthermals. *Global and Planetary Change* **170**, 120–125.

Cui Y., Schubert B. A. and Jahren A. H. (2020) A 23 my record of low atmospheric CO2. *Geology* **48**(9), 888–892.

De Boer H. J., Eppinga M. B., Wassen M. J. and Dekker S. C. (2012) A critical transition in leaf evolution facilitated the Cretaceous angiosperm revolution. *Nature Communications* **3**(1), 1–11.

Diefendorf A. F., Freeman K. H. and Wing S. L. (2012) Distribution and carbon isotope patterns of diterpenoids and triterpenoids in modern temperate C3 trees and their geochemical significance. *Geochimica et Cosmochimica Acta* **85**, 342–356.

Diefendorf A. F., Freeman K. H., Wing S. L., Currano E. D. and Mueller K. E. (2015) Paleogene plants fractionated carbon isotopes similar to modern plants. *Earth and Planetary Science Letters* **429**, 33–44.

Diefendorf A. F., Leslie A. B. and Wing S. L. (2019) A phylogenetic analysis of conifer diterpenoids and their carbon isotopes for chemotaxonomic applications. *Organic Geochemistry* **127**, 50–58.

Diefendorf A. F., Mueller K. E., Wing S. L., Koch P. L. and Freeman K. H. (2010) Global patterns in leaf 13C discrimination and implications for studies of past and future climate. *Proceedings of the National Academy of Sciences* **107**(13), 5738–5743.

Eberle J. J. and Greenwood D. R. (2012) Life at the top of the greenhouse Eocene world—A review of the Eocene flora and vertebrate fauna from Canada's High Arctic. *Bulletin* **124**(1-2), 3–23.

Ehleringer J., R, Hall A. E. and Farquhar G. D. (1993). Water use in relation to productivity, Chapter in Saugier et al (Eds.), Stable isotopes and plant carbon-water relations, Elsevier, pp. 155–172.

Farquhar G. D. and Cernusak L. A. (2012) Ternary effects on the gas exchange of isotopologues of carbon dioxide. *Plant, Cell & Environment* **35**(7), 1221–1231.

Farquhar G. D., O'Leary M. H. and Berry J. A. (1982) On the relationship between carbon isotope discrimination and the intercellular carbon dioxide concentration in leaves. *Functional Plant Biology* **9**(2), 121–137.

Farquhar G. v., von Caemmerer S. v. and Berry J. (1980) A biochemical model of photosynthetic $CO_2$ assimilation in leaves of C3 species. *Planta* **149**(1), 78–90.

Flexas J. and Carriquí M. (2020) Photosynthesis and photosynthetic efficiencies along the terrestrial plant's phylogeny: Lessons for improving crop photosynthesis. *The Plant Journal* **101**(4), 964–978.

Foster G. L., Royer D. L. and Lunt D. J. (2017) Future climate forcing potentially without precedent in the last 420 million years. *Nature communications* **8**, 14845.

Frank D., Poulter B., Saurer M., Esper J., Huntingford C., Helle G., Treydte K., Zimmermann N. E., Schleser G., Ahlström A. *et al.* (2015) Water-use efficiency and transpiration across European forests during the Anthropocene. *Nature Climate Change* **5**(6), 579–583.

Franks P. J., Royer D. L., Beerling D. J., Van de Water P. K., Cantrill D. J., Barbour M. M. and Berry J. A. (2014) New constraints on atmospheric CO2 concentration for the Phanerozoic. *Geophysical Research Letters* **41**(13), 4685–4694.

Galmés J., Hermida-Carrera C., Laanisto L. and Niinemets Ü. (2016) A compendium of temperature responses of Rubisco kinetic traits: variability among and within photosynthetic groups and impacts on photosynthesis modeling. *Journal of experimental botany* **67**(17), 5067–5091.

Gehler A., Gingerich P. D. and Pack A. (2016) Temperature and atmospheric CO2 concentration estimates through the PETM using triple oxygen isotope analysis of mammalian bioapatite. *Proceedings of the National Academy of Sciences* **113**(28), 7739–7744.

Gessler A., Ferrio J. P., Hommel R., Treydte K., Werner R. A. and Monson R. K. (2014) Stable isotopes in tree rings: towards a mechanistic understanding of isotope fractionation and mixing processes from the leaves to the wood. *Tree physiology* **34**(8), 796–818.

Ghashghaie J., Badeck F.-W., Lanigan G., Nogués S., Tcherkez G., Deléens E., Cornic G. and Griffiths H. (2003) Carbon isotope fractionation during dark respiration and photorespiration in C3 plants. *Phytochemistry reviews* **2**(1-2), 145–161.

Graven H., Allison C. E., Etheridge D. M., Hammer S., Keeling R. F., Levin I., Meijer H. A., Rubino M., Tans P. P., Trudinger C. M. *et al.* (2017) Compiled records of carbon isotopes in atmospheric CO2 for historical simulations in CMIP6. *Geoscientific Model Development (Online)* **10**(12).

Greenwood D. R., Basinger J. F. and Smith R. Y. (2010) How wet was the Arctic Eocene rain forest? Estimates of precipitation from Paleogene Arctic macrofloras. *Geology* **38**(1), 15–18.

Guerrieri R., Belmecheri S., Ollinger S. V., Asbjornsen H., Jennings K., Xiao J., Stocker B. D., Martin M., Hollinger D. Y., Bracho-Garrillo R. *et al.* (2019) Disentangling the role of photosynthesis and stomatal conductance on rising forest water-use efficiency. *Proceedings of the National Academy of Sciences* **116**(34), 16909–16914.

Guerrieri R., Lepine L., Asbjornsen H., Xiao J. and Ollinger S. V. (2016) Evapotranspiration and water use efficiency in relation to climate and canopy nitrogen in US forests. *Journal of Geophysical Research: Biogeosciences* **121**(10), 2610–2629.

Haario H., Laine M., Mira A. and Saksman E. (2006) DRAM: efficient adaptive MCMC. *Statistics and computing* **16**(4), 339–354.

Hare V. J., Loftus E., Jeffrey A. and Ramsey C. B. (2018) Atmospheric CO2 effect on stable carbon isotope composition of terrestrial fossil archives. *Nature communications* **9**(1), 1–8.

Harris I., Jones P. D., Osborn T. J. and Lister D. H. (2014) Updated high-resolution grids of monthly climatic observations–the CRU TS3. 10 Dataset. *International journal of climatology* **34**(3), 623–642.

Helliker B. R. and Richter S. L. (2008) Subtropical to boreal convergence of tree-leaf temperatures. *Nature* **454**(7203), 511–514.

Hollis C. J., Dunkley Jones T., Anagnostou E., Bijl P. K., Cramwinckel M. J., Cui Y., Dickens G. R., Edgar K. M., Eley Y., Evans D. *et al.* (2019) The DeepMIP contribution to PMIP4: methodologies for selection, compilation and analysis of latest Paleocene and early Eocene climate proxy data, incorporating version 0.1 of the DeepMIP database. *Geoscientific Model Development* **12**(7), 3149–3206.

Kattge J., Bönisch G., Díaz S., Lavorel S., Prentice I. C., Leadley P., Tautenhahn S., Werner G. D., Aakala T., Abedi M. *et al.* (2020) TRY plant trait database–enhanced coverage and open access. *Global change biology* .

Keeling R. F., Graven H. D., Welp L. R., Resplandy L., Bi J., Piper S. C., Sun Y., Bollenbacher A. and Meijer H. A. (2017) Atmospheric evidence for a global secular increase in carbon isotopic discrimination of land photosynthesis. *Proceedings of the National Academy of Sciences* **114**(39), 10361–10366.

Köhler P., Nehrbass-Ahles C., Schmitt J., Stocker T. F. and Fischer H. (2017) A 156 kyr smoothed history of the atmospheric greenhouse gases CO2, CH4, and N2O and their radiative forcing. *Earth System Science Data* **9**(1), 363–387.

Kohn M. J. (2010) Carbon isotope compositions of terrestrial C3 plants as indicators of (paleo)ecology and (paleo)climate. *Proceedings of the National Academy of Sciences* **107**(46), 19691–19695.

Konrad W., Royer D. L., Franks P. J. and Roth-Nebelsick A. (2020) Quantitative critique of leaf-based paleo-CO2 proxies: Consequences for their reliability and applicability. *Geological Journal* .

Lavergne A., Graven H., De Kauwe M. G., Keenan T. F., Medlyn B. E. and Prentice I. C. (2019) Observed and modelled historical trends in the water-use efficiency of plants and ecosystems. *Global change biology* **25**(7), 2242–2257.

Lavergne A., Sandoval D., Hare V. J., Graven H. and Prentice I. C. (2020b) Impacts of soil water stress on the acclimated stomatal limitation of photosynthesis: insights from stable carbon isotope data. *Global Change Biology* **26**, 7158–7172.

Lavergne A., Voelker S., Csank A., Graven H., de Boer H. J., Daux V., Robertson I., Dorado-Liñán I., Martínez-Sancho E., Battipaglia G. *et al.* (2020a) Historical changes in the stomatal limitation of photosynthesis: empirical support for an optimality principle. *New Phytologist* **225**(6), 2484–2497.

Leavitt S. (2001) Seasonal response of $\delta^{13}$C in Pinus resinosa Ait. seedling growth rings to changing environment in controlled growth experiments. *Dendrochronologia* **19**(1), 9–22.

Leavitt S. and Newberry T. (1992) Systematics of stable-carbon isotopic differences between gymnosperm and angiosperm trees. *Plant Physiol.(Life Sci. Adv.)* **11**, 257–262.

Mills B. J., Belcher C. M., Lenton T. M. and Newton R. J. (2016) A modeling case for high atmospheric oxygen concentrations during the Mesozoic and Cenozoic. *Geology* **44**(12), 1023–1026.

Orr D. J., Alcântara A., Kapralov M. V., Andralojc P. J., Carmo-Silva E. and Parry M. A. (2016) Surveying Rubisco diversity and temperature response to improve crop photosynthetic efficiency. *Plant Physiology* **172**(2), 707–717.

Pedentchouk N., Sumner W., Tipple B. and Pagani M. (2008) $\delta$13C and $\delta$D compositions of n-alkanes from modern angiosperms and conifers: an experimental set up in central Washington State, USA. *Organic Geochemistry* **39**(8), 1066–1071.

Porter A. S., Gerald C. E.-F., McElwain J. C., Yiotis C. and Elliott-Kingston C. (2015) How well do you know your growth chambers? Testing for chamber effect using plant traits. *Plant Methods* **11**(1), 1–10.

Porter A. S., Gerald C. E.-F., Yiotis C., Montanez I. P. and McElwain J. C. (2019) Testing the accuracy of new paleoatmospheric CO2 proxies based on plant stable carbon isotopic composition and stomatal traits in a range of simulated paleoatmospheric O2:CO2 ratios. *Geochimica et Cosmochimica Acta* **259**, 69–90.

Porter A. S., Yiotis C., Montañez I. P. and McElwain J. C. (2017) Evolutionary differences in $\Delta^{13}$C detected between spore and seed bearing plants following exposure to a range of atmospheric $O_2$:$CO_2$ ratios; implications for paleoatmosphere reconstruction. *Geochimica et Cosmochimica Acta* **213**, 517–533.

Prentice I. C., Dong N., Gleason S. M., Maire V. and Wright I. J. (2014) Balancing the costs of carbon gain and water transport: testing a new theoretical framework for plant functional ecology. *Ecology Letters* **17**(1), 82–91.

Reich P. B., Hobbie S. E., Lee T. D. and Pastore M. A. (2018) Unexpected reversal of C3 versus C4 grass response to elevated $CO_2$ during a 20-year field experiment. *Science* **360**(6386), 317–320.

Reichgelt T., D'Andrea W. J., Valdivia-McCarthy A. d. C., Fox B. R., Bannister J. M., Conran J. G., Lee W. G. and Lee D. E. (2020) Elevated $CO_2$, increased leaf-level productivity, and water-use efficiency during the early Miocene. *Climate of the Past* **16**(4), 1509–1521.

Royer D. L., Moynihan K. M., McKee M. L., Londoño L. and Franks P. J. (2019) Sensitivity of a leaf gas-exchange model for estimating paleoatmospheric $CO_2$ concentration. *Climate of the Past* **15**(2).

Sakamoto A. and Murata N. (2002) The role of glycine betaine in the protection of plants from stress: clues from transgenic plants. *Plant, Cell & Environment* **25**(2), 163–171.

Schlanser K. M., Diefendorf A. F., West C. K., Greenwood D. R., Basinger J. F., Meyer H. W., Lowe A. J. and Naake H. H. (2020a) Conifers are a major source of sedimentary leaf wax n-alkanes when dominant in the landscape: Case studies from the Paleogene. *Organic Geochemistry* **147**, 104069.

Schouten S., Woltering M., Rijpstra W. I. C., Sluijs A., Brinkhuis H. and Damsté J. S. S. (2007) The Paleocene–Eocene carbon isotope excursion in higher plant organic matter: Differential fractionation of angiosperms and conifers in the Arctic. *Earth and Planetary Science Letters* **258**(3-4), 581–592.

Schubert B. A. and Jahren A. H. (2012) The effect of atmospheric $CO_2$ concentration on carbon isotope fractionation in C3 land plants. *Geochimica et Cosmochimica Acta* **96**, 29–43.

Schubert B. A. and Jahren A. H. (2018) Incorporating the effects of photorespiration into terrestrial paleoclimate reconstruction. *Earth-Science Reviews* **177**, 637–642.

Sheldon N. D., Smith S. Y., Stein R. and Ng M. (2020) Carbon isotope ecology of gymnosperms and implications for paleoclimatic and paleoecological studies. *Global and Planetary Change* **184**, 103060.

Sherwood S., Webb M. J., Annan J. D., Armour K. C., Forster P. M., Hargreaves J. C., Hegerl G., Klein S. A., Marvel K. D., Rohling E. J., Watanabe M., Andrews T., Braconnot P., Bretherton C. S., Foster G. L., Hausfather Z., Heydt A. S. v. d., Knutti R., Mauritsen T., Norris J. R., Proistosescu C., Rugenstein M., Schmidt G. A., Tokarska K. B. and Zelinka M. D. (2020) An assessment of Earth's climate sensitivity using multiple lines of evidence. *Reviews of Geophysics* **n/a**(n/a), e2019RG000678. e2019RG000678 2019RG000678.
**URL:** *https://agupubs.onlinelibrary.wiley.com/doi/abs/10.1029/2019RG000678*

Soh W. K., Yiotis C., Murray M., Parnell A., Wright I. J., Spicer R. A., Lawson T., Caballero R. and McElwain J. C. (2019) Rising $CO_2$ drives divergence in water use efficiency of evergreen and deciduous plants. *Science Advances* **5**(12), eaax7906.

Steinthorsdottir M., Jardine P. and Rember W. (2020) Near-Future $pCO_2$ during the hot Mid Miocene Climatic Optimum. *Paleoceanography and Paleoclimatology* p. e2020PA003900.

Stuiver M. and Braziunas T. F. (1987) Tree cellulose 13C/12C isotope ratios and climatic change. *Nature* **328**(6125), 58–60.

Tcherkez G. (2006) How large is the carbon isotope fractionation of the photorespiratory enzyme glycine decarboxylase? *Functional Plant Biology* **33**(10), 911–920.

Ubierna N., Cernusak L. A., Holloway-Phillips M., Busch F. A., Cousins A. B. and Farquhar G. D. (2019) Critical review: incorporating the arrangement of mitochondria and chloroplasts into models of photosynthesis and carbon isotope discrimination. *Photosynthesis research* **141**(1), 5–31.

Ubierna N. and Farquhar G. D. (2014) Advances in measurements and models of photosynthetic carbon isotope discrimination in C3 plants. *Plant, cell & environment* **37**(7), 1494–1498.

Voelker S. L., Brooks J. R., Meinzer F. C., Anderson R., Bader M. K.-F., Battipaglia G., Becklin K. M., Beerling D., Bert D., Betancourt J. L. *et al.* (2016) A dynamic leaf gas-exchange strategy is conserved in woody plants under changing ambient CO2: Evidence from carbon isotope discrimination in paleo and $CO_2$ enrichment studies. *Global change biology* **22**(2), 889–902.

Vogado N. O., Winter K., Ubierna N., Farquhar G. D. and Cernusak L. A. (2020) Directional change in leaf dry matter $\delta^{13}C$ during leaf development is widespread in $C_3$ plants. *Annals of Botany* .

Walker B. J., Orr D. J., Carmo-Silva E., Parry M. A., Bernacchi C. J. and Ort D. R. (2017) Uncertainty in measurements of the photorespiratory CO2 compensation point and its impact on models of leaf photosynthesis. *Photosynthesis research* **132**(3), 245–255.

694 Wang H., Prentice I. C., Keenan T. F., Davis T. W., Wright I. J., Cornwell W. K., Evans B. J. and Peng C.
695 (2017) Towards a universal model for carbon dioxide uptake by plants. *Nature plants* **3**(9), 734.

696 West C. K., Greenwood D. R. and Basinger J. F. (2015) Was the Arctic Eocene 'rainforest' monsoonal? Estimates
697 of seasonal precipitation from early Eocene megafloras from Ellesmere Island, Nunavut. *Earth and Planetary*
698 *Science Letters* **427**, 18–30.

699 Yiotis C. and McElwain J. C. (2019) A novel hypothesis for the role of photosynthetic physiology in shaping
700 macroevolutionary patterns. *Plant physiology* **181**(3), 1148–1162.

701 Zanne A. E., Tank D. C., Cornwell W. K., Eastman J. M., Smith S. A., FitzJohn R. G., McGlinn D. J., O'Meara B. C.,
702 Moles A. T., Reich P. B. *et al.* (2014) Three keys to the radiation of angiosperms into freezing environments.
703 *Nature* **506**(7486), 89–92.

704 Zhang H.-Y., Hartmann H., Gleixner G., Thoma M. and Schwab V. F. (2019) Carbon isotope fractionation
705 including photosynthetic and post-photosynthetic processes in C3 plants: Low [CO2] matters. *Geochimica et*
706 *Cosmochimica Acta* **245**, 1–15.

# Differences in carbon isotope discrimination between angiosperm and gymnosperm woody plants, and their relationship to atmospheric $O_2$:$CO_2$ ratio, physiology, and environment

(ELECTRONIC ANNEX)

Vincent J. Hare[1]
*Stable Light Isotope Laboratory, Department of Archaeology, University of Cape Town*
*Carbon Cycle Research Group, Department of Physics, Imperial College London*

Aliénor Lavergne
*Carbon Cycle Research Group, Department of Physics, Imperial College London*

(Dated: December 9, 2020)

[1]Email: vincent.john.hare@gmail.com

## 1 Locations of $\Delta^{13}C$ dataset

Figure S1 shows the location of the tree ring and leaf data sites for angiosperm and gymnosperm plants used in the study. The isotopic data are derived from diverse species and plant functional types growing in a wide range of environments characterised by different soil water content and evaporative demand (vapour pressure deficit, $D$, ranging around 0.1 and 2 kPa).

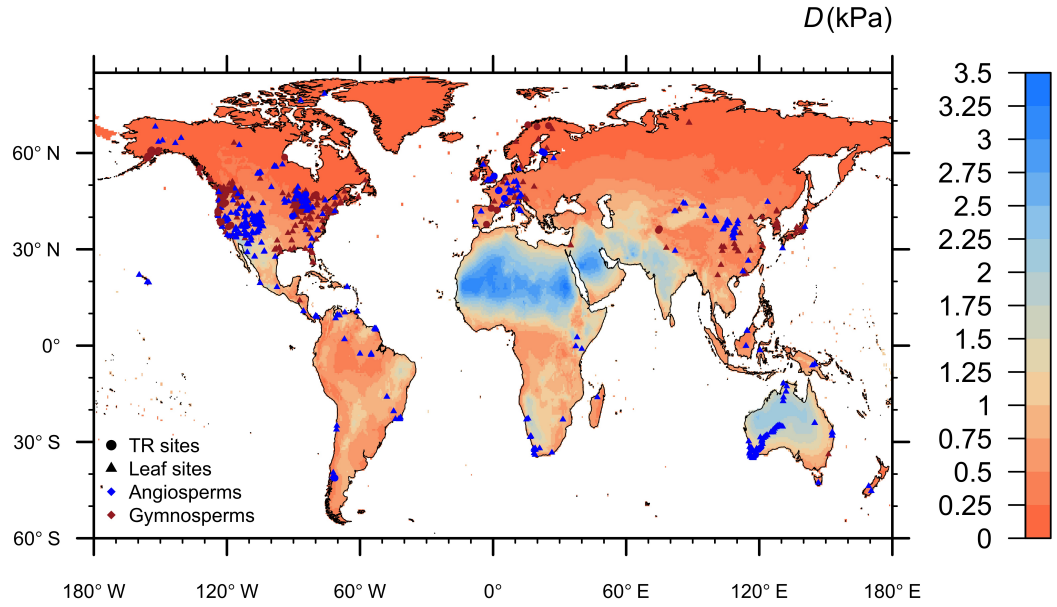


Figure S1: Global locations of tree ring (TR) and leaf stable carbon isotopic data. Blue points correspond to angiosperms, while red points are for gymnosperms. Yearly-averaged daytime vapour pressure deficit ($D$) is given in kPa.

## 2 Derivation of expression for $\Delta^{13}C$ in $C_c$-basis (Eq. 4, main text)

An comprehensive expression for leaf carbon isotope discrimination, assuming finite mesophyll conductance, and including photorespiration terms (but excluding fractionation during respiration), was proposed by [14] as:

$$\Delta^{13}\mathrm{C} = a_\mathrm{s}(1-\chi) + a_\mathrm{m}(\chi - \chi_\mathrm{c}) + b\chi_\mathrm{c} - (f - wh)\frac{\Gamma^*}{C_\mathrm{a}} \tag{2.1}$$

where for convenience we adopt the notation suggested by ref. [16] of $\chi = C_\mathrm{i}/C_\mathrm{a}$, and $\chi_\mathrm{c} = C_\mathrm{c}/C_\mathrm{a}$. Assuming that the $CO_2$ flux from the outside of the leaf to the intercellular spaces is equal to the flux from the intercelullar spaces to the chloroplast, Fick's law yields:

$$A = g_\mathrm{s}(C_\mathrm{a} - C_\mathrm{i}) = g_\mathrm{m}(C_\mathrm{i} - C_\mathrm{c}) \tag{2.2}$$

which can be rewritten as:

$$g_\mathrm{s}(1-\chi) = \theta_\mathrm{m} g_\mathrm{s}(\chi - \chi_\mathrm{c}) \tag{2.3}$$

where $\theta_\mathrm{m}$ is the ratio of mesophyll ($g_\mathrm{m}$) to stomatal conductance ($g_\mathrm{s}$). Rearranging this expression yields

$$(1-\chi) = \frac{\theta_\mathrm{m}(1-\chi_\mathrm{c})}{1+\theta_\mathrm{m}}\ , \text{ and} \tag{2.4}$$

$$(\chi - \chi_{\mathrm{c}}) = \frac{1 - \chi_{\mathrm{c}}}{1 + \theta_{\mathrm{m}}} \tag{2.5}$$

Inserting Eqns 1.4-1.5 into Eq. 1.1 yields the expression for $\Delta^{13}\mathrm{C}$ in terms of $\chi_{\mathrm{c}}$:

$$\Delta^{13}\mathrm{C} = \bar{a} + \big[b - \bar{a}\big]\chi_{\mathrm{c}} - f\frac{\Gamma_{\mathrm{c}}}{C_{\mathrm{a}}} \tag{2.6}$$

where $\bar{a} = (a_{\mathrm{s}}\theta_{\mathrm{m}} + a_{\mathrm{m}})/(1 + \theta_{\mathrm{m}})$.

## 3 Rubisco kinetics

Parameters associated with Rubisco kinetics include the Michaelis-Menten coefficients for $CO_2$, $K_{\mathrm{c}}$ (Pa), and $O_2$, $K_{\mathrm{o}}$ (Pa), as well as $\Gamma_{\mathrm{c}}$ (Pa). The former two parameters are combined into the effective Michaelis-Menten coefficient for Rubisco, $K$ (Pa), as follows:

$$K = K_{\mathrm{c}}\big(1 + \frac{p\mathrm{O}_2}{K_{\mathrm{o}}}\big) \tag{3.1}$$

Both $K_{\mathrm{c}}$ and $K_{\mathrm{o}}$ exhibit an Arrhenius temperature response which depends on their respective activation energies ($E_{\mathrm{a,Kc}}$ and $E_{\mathrm{a,Ko}}$). At any given temperature T (K), these variables in (Pa) were computed as follows:

$$K_{\mathrm{c}}(\mathrm{T}) = K_{\mathrm{c},25} \times 10^{-6} P_{\mathrm{atm}} \exp\big[\frac{E_{\mathrm{a,Kc}}}{R}(\frac{1}{298.15} - \frac{1}{T})\big] \tag{3.2}$$

$$K_{\mathrm{o}}(\mathrm{T}) = K_{\mathrm{o},25} \times 10^{-3} P_{\mathrm{atm}} \exp\big[\frac{E_{\mathrm{a,Ko}}}{R}(\frac{1}{298.15} - \frac{1}{T})\big] \tag{3.3}$$

Values for $K_{\mathrm{c},25}$, $E_{\mathrm{a,Kc}}$, $K_{\mathrm{o},25}$, and $E_{\mathrm{a,Ko}}$ were taken from study [1] as 272.38 $\mu$mol mol$^{-1}$, 80.99 kJ mol$^{-1}$, 165.82 mmol mol$^{-1}$, and 23.72 kJ mol$^{-1}$ respectively. For leaf and tree ring data, $p\mathrm{O}_2$ was estimated from altitude ($z$, in meters) via a standard barometric formula:

$$p\mathrm{O}_2\ [\mathrm{Pa}]\ = 101325 \times (1 - (2.25577 \times 10^{-5})z)^{5.25588} \tag{3.4}$$

Finally, the photorespiratory $CO_2$ compensation point (Pa) was calculated as:

$$\Gamma_{\mathrm{c}}(T) = \Gamma_{\mathrm{c},25} \times 10^{-6} P_{\mathrm{atm}} \big(\lambda/\lambda_{\mathrm{ref}}\big) \exp\big[\frac{E_{\mathrm{a},\Gamma_{\mathrm{c}}}}{R}(\frac{1}{298.15} - \frac{1}{T})\big] \tag{3.5}$$

Likewise, $\Gamma_{\mathrm{c},25}$ and $E_{\mathrm{a},\Gamma_{\mathrm{c}}}$ were taken from [1] as 37.43 $\mu$mol mol$^{-1}$ and 24.46 kJ mol$^{-1}$. Since these values were estimated for tobacco at 25$^o$C, we use the $\lambda_{\mathrm{ref}}$ value inferred from [15] as 0.6.

## 4 Estimation of daytime growing leaf temperature, $T_{\mathrm{d}}$

Latitude and longitude were used to extract minimum and maximum temperatures ($T_{\mathrm{min}}$ and $T_{\mathrm{min}}$, $^o$C), and actual vapor pressure ($e_{\mathrm{a}}$) for each site from monthly 0.5$^o$ resolution data provided by the Climatic

Research Unit (CRU Ts4.03; Ref. [9]). We calculated the raw monthly mean daytime air $T$ ($T_{\mathrm{d,raw}}$) to consider only the part of the day when photosynthesis occurs, as:

$$T_{\mathrm{d,raw}} = T_{\mathrm{max}}\left[\frac{1}{2} + \frac{\sqrt{1-x^2}}{2\mathrm{arccos}x}\right] + T_{\mathrm{min}}\left[\frac{1}{2} - \frac{\sqrt{1-x^2}}{2\mathrm{arccos}x}\right] \tag{4.1}$$

where $x = -\mathrm{tan}\phi\mathrm{tan}\delta$, with $\phi$ the latitude, and $\delta$ the average solar declination for the month.

We then convert raw monthly mean daytime air temperature to rough estimation of leaf temperature, $T_{\mathrm{d}}$, using the relationship identified between mean daytime air temperature (growing season) and leaf temperature in [10] (illustrated in Figure S2, S3). A regression was perfomed on the [10] data, excluding outlier values for the high Arctic (shown in red). The regression yielded a slope of 0.2998, and an intercept of 15.287 $^o$C ($R^2$ = 0.3). This attenuates the variation in the raw values, to a range between 12 and 23 $^o$C (e.g. for gymnosperms, shown below).

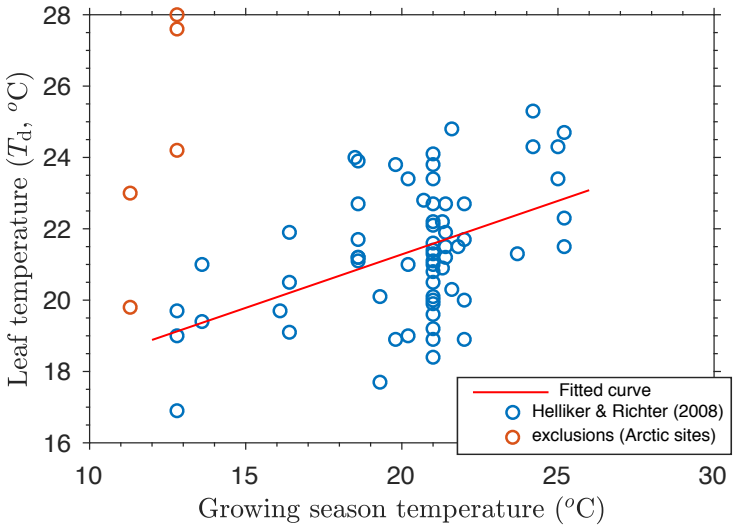


Figure S2: MCMC chains for estimation of angiosperm parameters (leaf + tree ring).

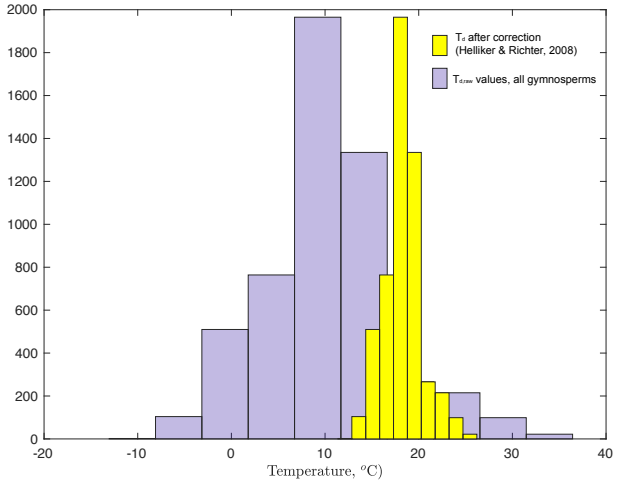


Figure S3: Comparison of raw (purple) and corrected (yellow) daytime leaf growing temperatures, after correction using the regressed relationship in Figure S2)

## 5 Full list of symbols used

| Variable (units) | Description | Reference |
|---|---|---|
| $\Delta^{13}$C (‰) | leaf-level carbon isotope discrimination | [14, 13, 3] |
| $\Delta^{13}C_a$ (‰) | leaf-level carbon isotope discrimination, average angiosperm | *this study* |
| $\Delta^{13}C_g$ (‰) | leaf-level carbon isotope discrimination, average gymnosperm | *this study* |
| $\Delta^{13}C^*_{a-g}$ (‰) | difference between average co-located angiosperm and gymnosperm $\Delta^{13}$C at constant $T_d$, $P_{atm}$, & $D$ | *this study* |
| $\varepsilon_{lipid}$ (‰) | post-photosynthetic fractionation during biosynthesis of leaf lipids | |
| $\varepsilon_{cellulose}$ (‰) | post-photosynthetic fractionation during biosynthesis of cellulose | |
| $t$ | ternary correction factor | [14, 13, 3] |
| $a_s$ (‰) | fractionation for $CO_2$ diffusion in air, 4.4‰ | [5] |
| $a_m$ (‰) | fractionation for $CO_2$ diffusion in water, 1.8‰ | [14] |
| $b$ (‰) | fractionation during Rubisco carboxylation, 30‰ | [14] |
| $f$ (‰) | fractionation during photorespiration, 8-18‰ (theoretical: 11‰) | [12] |
| $h$ (‰) | apparent fractionation resulting from starch formation, and/or the kinetic fractionation associated with the export of triose phosphates (TP) from the chloroplast, and/or enzymes such as aldolase, transaldolase, transketolase and TP isomerase | [3] |
| $w$ (unitless) | coefficient of $h$ in $f - wh$ | [3] |
| $\alpha_b$ (unitless) | fractionation factor for $^{13}$C/$^{12}$C during carboxylation, $\alpha_b = 1 + b$ | [14] |
| $\alpha_e$ (unitless) | fractionation factor for $^{13}$C/$^{12}$C during respiration, $\alpha_b = 1 + e$ | [14] |
| $\alpha_f$ (unitless) | fractionation factor for $^{13}$C/$^{12}$C during photorespiration, $\alpha_b = 1 + f$ | [14] |
| $\alpha_h$ (unitless) | as above, for $h$ | [3] |
| $\lambda$ (unitless) | amount of $CO_2$ released from photorespiration per oxygenation reaction, relative to that of *N. tabacum* at 25°C | [2] |
| $\lambda_a$ (unitless) | average $\lambda$, woody angiosperms | *this study* |
| $\lambda_g$ (unitless) | average $\lambda$, woody gymnosperms | *this study* |
| $\varepsilon_f$ (unitless) | gradient of the slope of $\Delta^{13}C^*_{a-g}$ vs $[O_2]/[CO_2]$ at constant $T_d$, $D$. | *this study* |
| $\varepsilon_{ab}$ (unitless) | intercept of the slope of $\Delta^{13}C^*_{a-g}$ vs $[O_2]/[CO_2]$ at constant $T_d$, $D$. | *this study* |
| $\alpha_G$ (unitless) | proportion of glycine removed from the photorespiratory pathway | [4, 2] |
| $\alpha_T$ (unitless) | proportion of 2-Phosphoglycolate carbon exported as $CH_2$-THF from the photorespiratory pathway | [2] |
| $C_a$ (Pa) | atmospheric $pCO_2$ (Pa), or as concentration ($\mu$mol mol$^{-1}$) | |
| $C_s$ (Pa) | leaf-surface $pCO_2$ (Pa), or as concentration ($\mu$mol mol$^{-1}$) | |
| $C_i$ (Pa) | leaf intercellular $pCO_2$ (Pa), or as concentration ($\mu$mol mol$^{-1}$) | |
| $C_c$ (Pa) | chloroplastic $pCO_2$ (Pa), or as concentration ($\mu$mol mol$^{-1}$) | |
| $O_c$ (mol.mol$^{-1}$) | chloroplastic oxygen concentration | |
| $g_s$ (mol m$^{-2}$ s$^{-1}$) | stomatal conductance | [6, 17] |
| $g_m$(mol m$^{-2}$ s$^{-1}$) | mesophyll conductance | [6, 17] |
| $\beta_c$ (unitless) | ratio of carboxylation to transpiration cost factors at 25 °C | [16] |
| $A$ (mol m$^{-2}$ s$^{-1}$) | net rate of $CO_2$ assimilation | |
| $\eta^*$ (unitless) | viscosity of water relative to its value at 25°C | [16] |
| $K_c$ (Pa) | Michaelis-Menten coefficient of Rubisco carboxylation | [1] |
| $K_o$ (Pa) | Michaelis-Menten coefficient of Rubisco oxygenation | [1] |
| $K$ (Pa) | effective Michaelis-Menten coefficient of Rubisco | [1] |
| $S_{c/o}$ (mol mol$^{-1}$) | Rubisco $CO_2$/$O_2$ specificity | [7] |
| $\Gamma_c$ (Pa) | chloroplastic $CO_2$ compensation point in the absence of mitochondrial respiration, when $A = 0$ | [13] |
| $\Gamma^*$ (Pa) | chloroplastic $CO_2$ compensation point in the absence of mitochondrial respiration, when $A = -\mathcal{R}_d$ | [13] |
| $z$ (m) | elevation | |
| $P_{atm}$ (kPa) | atmospheric pressure | |
| $T_d$ (°K) | daytime leaf temperature | |
| $D$ (kPa) | daytime vapour pressure deficit | |
| $[O_2]$ (mol mol$^{-1}$) | atmospheric oxygen concentration | |
| $[CO_2]$ (mol mol$^{-1}$) | atmospheric carbon dioxide concentration | |

Note: Partial pressure and concentration are equivalent in equations for $\Delta^{13}$C when used in $\chi$ or $\chi_c$ terms, but when $C_a$ appears as the denominator, e.g. $\Gamma^*/C_a$, the units should match that of $\Gamma^*$.

## 6 Fitting procedure

We employed a Markov chain Monte Carlo technique (MCMC) based on the delayed rejection adaptive Metropolis (DRAM) algorithm of ref. [8] for robust parameter estimation of $\beta_{\mathrm{c}}$, $g_{\mathrm{m}}/g_{\mathrm{s}}$, and $\lambda/\lambda_{\mathrm{ref}}$. All MATLAB code is available from the authors.

We estimated these parameters for both combined and individual leaf and tree ring datasets. In all cases, we consider a model in the form of Eqns. (5-8), with Gaussian errors, and constants $b = 30$ ‰, $a_s = 4.4$ ‰, $a_m = 1.8$ ‰, $R = 8.3145$ J mol$^{-1}$ K$^{-1}$, and $f = 11 \pm 2$ ‰. Rubisco kinetic parameters were taken from [1], and computed as in Section 2. Parameters for angiosperms were modelled as:

$$\beta_{\mathrm{c}} \sim \text{Uniform(70,1000)}$$
$$g_{\mathrm{m}}/g_{\mathrm{s}} \sim \text{Norm}(\mu_1, {s_1}^2),\ g_{\mathrm{m}}/g_{\mathrm{s}} \in [0.06, 6.3]$$
$$\lambda/\lambda_{\mathrm{ref}} \sim \text{Uniform(0,10)}$$

Whereas parameters for gymnosperms were modelled as:

$$\beta_{\mathrm{c}} \sim \text{Uniform(70,1000)}$$
$$g_{\mathrm{m}}/g_{\mathrm{s}} \sim \text{Norm}(\mu_2, {s_2}^2),\ g_{\mathrm{m}}/g_{\mathrm{s}} \in [0.5, 4.3]$$
$$\lambda/\lambda_{\mathrm{ref}} \sim \text{Uniform(0,10)}$$

Our choice was motivated as follows. Constraints on the range of $\beta_{\mathrm{c}}$ (between 70 and 1000) were chosen in accordance to other analyses (e.g. [11, 16]), and are quite conservative. The range of $g_{\mathrm{m}}/g_{\mathrm{s}}$ was chosen to reflect the isotope-independent measurements reported in ref. [17], and initial values of $\mu_1$,$s_1$, $\mu_2$, and $s_2$ chosen from the same study as 1.8, 1.1, 0.9, and 0.1, respectively. $\lambda/\lambda_{ref}$ must be greater than 0, and is expected to be around 1. It could also be greater than 1 if the proportion of $CH_2$-THF exported from the photorespiratory pathway increases. Thus, we use a likely range of values between 0 and 10.

MCMC chains were run for 15000 iterations. To assess chain quality and algorithm convergence, we considered both integrated correlation time, $\tau$ (a measure of the averaged number of iterations required to achieve independent sampling), and a Geweke test (the output of which is equivalent to a Z-test). Lower $\tau$ values, and a Geweke statistic approaching 1 ($p << 0.05$) can be regarded as indications of acceptable chain convergence.

Figure S5 shows the chain outputs for the combined angiosperm datasets, as an example. All statistics can be found in Tables S1-S4. In all cases, chains converged rapidly on the stationary distribution ($\tau < 48$).

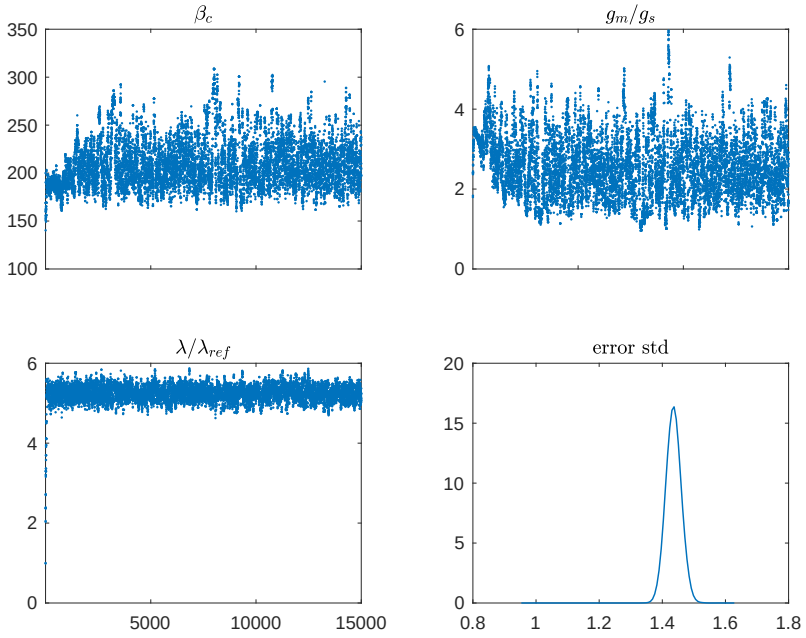


Figure S4: MCMC chains for estimation of angiosperm parameters (leaf + tree ring).

Table S1. Fitted parameters: angiosperm leaf $\Delta^{13}\mathrm{C}$ dataset.

| Parameter | $\mu$ | $\pm1\sigma$ | MC error | $\tau$ | Geweke |
|---|---|---|---|---|---|
| $\beta_\mathrm{c}$ | 214 | 26 | 1.9 | 48 | 0.89 |
| $g_\mathrm{m}/g_\mathrm{s}$ | 2.5 | 0.77 | 0.06 | 54 | 0.70 |
| $\lambda/\lambda_\mathrm{ref}$ | 5.2 | 0.31 | 0.02 | 58 | 0.95 |

Table S2. Fitted parameters: angiosperm tree ring $\Delta^{13}\mathrm{C}$ dataset.

| Parameter | $\mu$ | $\pm1\sigma$ | MC error | $\tau$ | Geweke |
|---|---|---|---|---|---|
| $\beta_\mathrm{c}$ | 284 | 25 | 0.6 | 20 | 0.99 |
| $g_\mathrm{m}/g_\mathrm{s}$ | 3.2 | 0.74 | 0.03 | 45 | 0.86 |
| $\lambda/\lambda_\mathrm{ref}$ | 4.8 | 0.3 | 0.01 | 31 | 0.96 |

Table S3. Fitted parameters: gymnosperm leaf $\Delta^{13}\mathrm{C}$ dataset.

| Parameter | $\mu$ | $\pm1\sigma$ | MC error | $\tau$ | Geweke |
|---|---|---|---|---|---|
| $\beta_\mathrm{c}$ | 346 | 40 | 3.6 | 107 | 0.85 |
| $g_\mathrm{m}/g_\mathrm{s}$ | 0.94 | 0.09 | 0.005 | 36 | 0.94 |
| $\lambda/\lambda_\mathrm{ref}$ | 7.3 | 0.75 | $9\times10^{-3}$ | 190 | 0.81 |

Table S4. Fitted parameters: gymnosperm tree ring $\Delta^{13}\mathrm{C}$ dataset

| Parameter | $\mu$ | $\pm1\sigma$ | MC error | $\tau$ | Geweke |
|---|---|---|---|---|---|
| $\beta_\mathrm{c}$ | 140 | 10 | 0.5 | 28 | 0.96 |
| $g_\mathrm{m}/g_\mathrm{s}$ | 0.89 | 0.10 | 0.006 | 34 | 0.91 |
| $\lambda/\lambda_\mathrm{ref}$ | 0.44 | 0.22 | $1\times10^{-2}$ | 27 | 0.70 |

## 7 Sensitivity analyses

In Section 4.1 of the main manuscript, we conducted sensitivity analyses across a range of $[O_2]$:$[CO_2]$ ratios from 200 (e.g. Palaeogene) to 1200 (e.g. LGM) using Eqns. (5-7) and our best-fitted values for $\beta_c$, $g_m/g_s$, and $\lambda/\lambda_{ref}$ at 20$^o$C, at two different levels of vapour pressure deficit. In fact, these simulations were a subset of a larger number of simulations over variable $D$ (shown in Fig S5a) and variable $T_d$ (shown in Fig. S5b). The MATLAB code is also available from the authors.

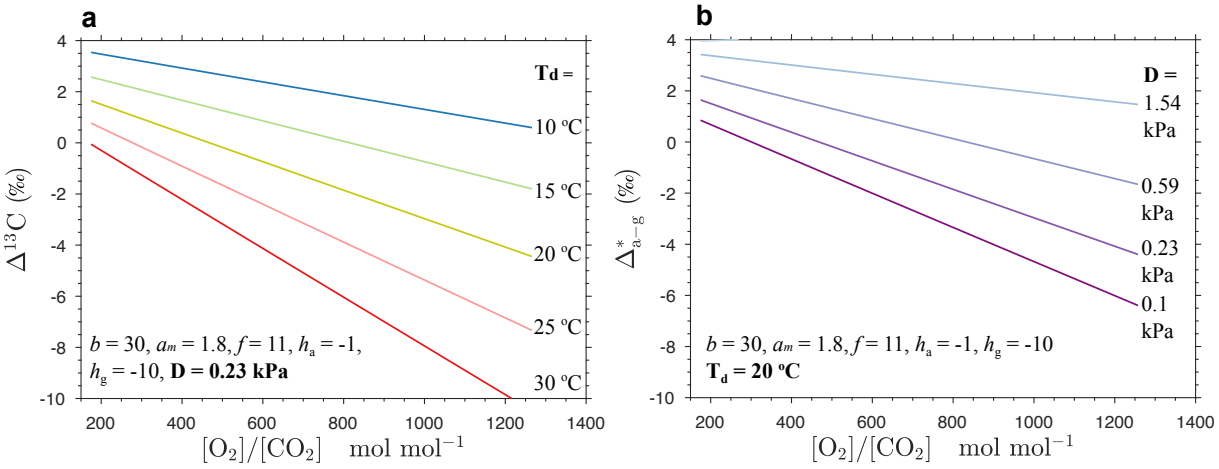


Figure S5: Simulations of the effects of $[O_2]$:$[CO_2]$ ratio on $\Delta^*_{a-g}$ for different environmental conditions, using parameters for plant specific traits ($\beta_c$, $g_m/g_s$, and $\lambda/\lambda_{ref}$). (a) shows the effect of variable $T$, at constant $D$, at two different scenarios for $\lambda/\lambda_{ref}$ (dashed and solid lines); and (b) shows the effect of variable $D$, at constant $T$, for the same scenarios of $\lambda/\lambda_{ref}$ as in (a).

These simulations show that $\Delta^*_{a-g}$ decrease with increasing $[O_2]$/$[CO_2]$ when $\lambda_a > \lambda_g$ (solid lines), and that the magnitude of this decrease is stronger with increasing $T$ and/or decreasing $D$ (the highest gradients are for $T = 30^o$C, and $D = 0.1$ kPa).

Our simulations also show that the $D$ effect is stronger than the $T$ effect, considering the range of leaf $T_d$ estimated according to Section 4 (above). $D$ levels higher than 1.5 kPa indicate significant water demand for transpiration. Note that because higher $D$ is usually also accompanied by higher temperatures, the two effects are expected to partly cancel each other out with respect to $\Delta^*_{a-g}$. However, the $D$ effect is much stronger, and ultimately wins!

## 8 Datasets

The following datasets are included in this paper, in excel format:

Global13Cdata.xlsx

Binned13Cdata.xlsx

(both available via link: https://doi.org/10.6084/m9.figshare.12722423.v1)

## References

[1] Carl J Bernacchi, Archie R Portis, Hiromi Nakano, Susanne von Caemmerer, and Stephen P Long. Temperature response of mesophyll conductance. implications for the determination of rubisco

enzyme kinetics and for limitations to photosynthesis in vivo. *Plant physiology*, 130(4):1992–1998, 2002.

[2] Florian A Busch. Photorespiration in the context of rubisco biochemistry, co2 diffusion, and metabolism. *The Plant Journal*, 2020.

[3] Florian A Busch, Meisha Holloway-Phillips, Hilary Stuart-Williams, and Graham D Farquhar. Revisiting carbon isotope discrimination in c 3 plants shows respiration rules when photosynthesis is low. *Nature Plants*, 6(3):245–258, 2020.

[4] Florian A Busch, Rowan F Sage, and Graham D Farquhar. Plants increase CO2 uptake by assimilating nitrogen via the photorespiratory pathway. *Nature plants*, 4(1):46, 2018.

[5] Harmon Craig. Carbon 13 in plants and the relationships between carbon 13 and carbon 14 variations in nature. *The journal of geology*, pages 115–149, 1954.

[6] Jaume Flexas and Marc Carriquí. Photosynthesis and photosynthetic efficiencies along the terrestrial plant's phylogeny: lessons for improving crop photosynthesis. *The Plant Journal*, 2019.

[7] Jeroni Galmés, Carmen Hermida-Carrera, Lauri Laanisto, and Ülo Niinemets. A compendium of temperature responses of rubisco kinetic traits: variability among and within photosynthetic groups and impacts on photosynthesis modeling. *Journal of experimental botany*, 67(17):5067–5091, 2016.

[8] Heikki Haario, Marko Laine, Antonietta Mira, and Eero Saksman. Dram: efficient adaptive mcmc. *Statistics and computing*, 16(4):339–354, 2006.

[9] IPDJ Harris, Philip D Jones, Timothy J Osborn, and David H Lister. Updated high-resolution grids of monthly climatic observations–the CRU TS3. 10 Dataset. *International journal of climatology*, 34(3):623–642, 2014.

[10] Brent R Helliker and Suzanna L Richter. Subtropical to boreal convergence of tree-leaf temperatures. *Nature*, 454(7203):511–514, 2008.

[11] Alienor Lavergne, David Sandoval, Vincent J Hare, Heather D Graven, and I Colin Prentice. Soil water stress impacts on the stomatal limitation of photosynthesis: a meta-analysis. *In Review, Global Change Biology*, 2020.

[12] Guillaume Tcherkez. How large is the carbon isotope fractionation of the photorespiratory enzyme glycine decarboxylase? *Functional Plant Biology*, 33(10):911–920, 2006.

[13] Nerea Ubierna, Lucas A Cernusak, Meisha Holloway-Phillips, Florian A Busch, Asaph B Cousins, and Graham D Farquhar. Critical review: incorporating the arrangement of mitochondria and chloroplasts into models of photosynthesis and carbon isotope discrimination. *Photosynthesis research*, 141(1):5–31, 2019.

[14] Nerea Ubierna and Graham D Farquhar. Advances in measurements and models of photosynthetic carbon isotope discrimination in c 3 plants. *Plant, cell & environment*, 37(7):1494–1498, 2014.

[15] Berkley J Walker, Douglas J Orr, Elizabete Carmo-Silva, Martin AJ Parry, Carl J Bernacchi, and Donald R Ort. Uncertainty in measurements of the photorespiratory co2 compensation point and its impact on models of leaf photosynthesis. *Photosynthesis research*, 132(3):245–255, 2017.

[16] Han Wang, I Colin Prentice, Trevor F Keenan, Tyler W Davis, Ian J Wright, William K Cornwell, Bradley J Evans, and Changhui Peng. Towards a universal model for carbon dioxide uptake by plants. *Nature plants*, 3(9):734, 2017.

[17] Charilaos Yiotis and Jennifer C McElwain. A novel hypothesis for the role of photosynthetic physiology in shaping macroevolutionary patterns. *Plant physiology*, 181(3):1148–1162, 2019.